学位論文（要約）

Studies of RAB GTPases in the basal land plant, *Marchantia polymorpha*

（基部陸上植物ゼニゴケの RAB GTPase の研究）

平成 29 年 12 月博士（理学）申請

東京大学大学院理学系研究科

生物科学専攻

南野　尚紀

Table of contents

Abstract

The RAB GTPase is an evolutionarily conserved machinery component of membrane trafficking, which is the fundamental system for cell viability and higher-order biological functions. The composition of RAB GTPases in each organism is closely related to the complexity and organization of the membrane-trafficking pathway, which has been developed uniquely to realize the organism-specific membrane trafficking system. Comparative genomics has suggested that diversification of the membrane trafficking system has been partly achieved by the increase in the number of RAB GTPases followed by functional diversification. Meanwhile, a considerable number of subgroups of RAB GTPases were secondarily lost during evolution, which suggests that secondary loss of RAB GTPases could be another method for specialization of the membrane trafficking system. However, it remains mostly unknown how novel acquisition and secondary loss of RAB GTPases were involved in evolution and diversification of the membrane trafficking system. To obtain insights into diversification of the membrane trafficking system during green plant evolution, I analyzed RAB GTPases encoded in the genome of the liverwort, *Marchantia polymorpha* in a comprehensive manner. I isolated all genes encoding RAB GTPases in *M. polymorpha* and analyzed their expression patterns and subcellular localizations in thallus cells. MpRAB2b, which contains a sequence similar to that of an intraflagellar transport protein at the carboxyl (C)-terminal region, is specifically expressed in the male reproductive organ. This type of RAB GTPases has not been identified in other organisms, suggesting that it was a uniquely acquired member of RAB GTPase in liverworts. Mp*RAB21*, whose homolog is absent in Arabidopsis thus this could be an example of secondarily lost RAB GTPases during plant evolution, exhibited endosomal localization with RAB5 members in *M. polymorpha*. Further functional

analyses revealed that MpRAB21 plays and essential role for normal thallus development of *M. polymorpha*, although most of angiosperms lost this RAB GTPase. Furthermore, I found that MpRAB21 could function in a secretory pathway from late endosomes. These results suggest that mechanisms of endosomal transport have been diverged among land plant species. I also demonstrated that in antheridia in the male reproductive organ, spermatozoids are generated through drastic reorganization of the plasma membrane and organelles including the Golgi apparatus and endosomes by live imaging. Intriguingly, the *RAB23* homolog in *M. polymorpha*, another example of secondarily lost RAB GTPases during plant evolution, is specifically required for spermatozoid functions. Genetic and cell biological analyses indicated that MpRAB23 is required for organizing microtubule-containing structures in spermatozoids including the axoneme in flagella. In a consistent manner, the distribution of the *RAB23* group in green plants is tightly correlated with the presence of flagella in male gametes. These results indicated that the loss of *RAB23* is associated with the evolution of male gamete motility in plants.

Acknowledgements

Abbreviations

BODIPY 493/503; 4,4-Difluoro-1,3,5,7,8-Pentamethyl-4-Bora-3a,4a-Diaza-*s*-Indacene

BSA; bovine serum albumin

CaMV; cauliflower mosaic virus

C-terminus; Carboxyl-terminus

EDTA; ethylene diamine tetraacetic acid

EGTA; ethylene glycol tetraacetic acid

EE; early endosome

ESCRT; endosomal sorting complex required for transport

FM1-43; *N*-(3-Triethylammoniumpropyl)-4-(4-(Dibutylamino) Styryl) Pyridinium Dibromide

GAP; GTPase activating protein

GEF; guanine nucleotide exchange factor

GMP-PNP; guanylyl imidodiphosphate

gRNA; guide RNA

GST; glutathione *S*-transferase

HEPES; *N*-2-hydroxyethylpiperazine-*N'*-2-ethane sulfonic acid

IFT; intraflagellar transport

Mant-GDP; 2'-(or-3')-*O*-(*N*-Methylanthraniloyl) Guanosine 5'-Diphosphate

MLS; multilayered structure

mGFP; monomeric green fluorescent protein

mRFP; monomeric red fluorescent protein

MS; mass spectrometry

MVE; multivesicular endosome

NLS; nuclear localization signal

ORF; open reading flame

PAM; protospacer adjacent motif

PO; propylene oxide

RT-PCR; reverse transcription PCR

PBS; phosphate buffer saline

PFA; paraformaldehyde

PIPES; Piperazine-1,4-bis(2-ethanesulfonic acid)

SDS; sodium lauryl sulfate

Shh; Sonic hedgehog

SNARE; soluble *N*-ethylmaleimide-sensitive factor attachment protein receptor

ST; sialyltransferase

TGN; *trans*-Golgi network

General introduction

Membrane trafficking is the fundamental system in eukaryotic cells for transporting proteins and lipids among single-membrane-bounded organelles and across the plasma membrane, and it plays a pivotal role in various fundamental and higher-order physiological phenomena, including development, stress response, and immunity. A single membrane trafficking event between donor and target organelles consists of several sequential processes, including 1) forming vesicles from the donor membrane, 2) transporting vesicles, 3) tethering vesicles to the target membrane, and 4) fusing the transport vesicles to the target membrane. These processes involve several highly conserved machinery components in eukaryotes, which include RAB GTPase (Figure 1A). RAB GTPase acts as a molecular switch by cycling between GTP-bound active and GDP-bound inactive forms, which is mediated by a guanine nucleotide exchange factor (GEF) and a GTPase-activating protein. Activated RAB GTPase interacts with a specific set of effector proteins, which evoke downstream reactions, including tethering of transport vesicles to the target membrane mediated by tethering factors (Figure 1B) (Fujimoto and Ueda, 2012; Grosshans et al., 2006; Hutagalung and Novick, 2011; Saito and Ueda, 2009). While RAB GTPase is a highly conserved machinery component essential for membrane trafficking, it has also been reported that each organism harbors a specific repertoire of RAB GTPases, suggesting that diversification and specialization of the set of RAB GTPases is tightly associated with diversification of the membrane trafficking system during evolution.

Comparative genomic analyses proposed that diversification of membrane trafficking system in the plant lineage could be associated with terrestrialization and multicellularization (Rutherford and Moore, 2002; Sanderfoot, 2007). However,

6

information from basal land plants is still limited to firmly conclude it. *Marchantia polymorpha* is the liverwort, which is one of the basalmost land plants (Figure 2). *M. polymorpha* is an emerging model plant, whose genome information and various genetic techniques are already available. In Chapter 1, I identified genes for RAB GTPases in the genome of *M. polymorpha*, and then examined expression patterns and subcellular localizations of all members of RAB GTPases in this plant. I demonstrated that *M. polymorpha* harbors some RAB GTPases with distinctive characteristics as well as a fundamental set of RAB GTPases shared with other green plants with low redundancy. Recent comparative genomics proposed that larger numbers of RAB subgroups were present in the last eukaryotic common ancestor (LECA), and many RAB GTPases were secondarily lost in the process of diversification of eukaryotic lineages (Elias et al., 2012; Klopper et al., 2012). It suggests that secondary loss of RAB GTPase would substantially contribute to the diversification and specialization of the membrane trafficking system. RAB21 and RAB23 in *M. polymorpha*, whose homologous products were secondarily lost in most of angiosperms including Arabidopsis, should be suitable targets to unravel the significance of secondary loss of RAB GTPases during land plant evolution. Furthermore, precise molecular functions of RAB21 and RAB23 remain unclear even in non-plant systems including animals. For insights into functions of these RAB GTPases in *M. polymorpha*, I performed functional analyses of MpRAB21 in Chapter 2, and revealed that MpRAB21 is involved in a trafficking pathway from endosomes probably to the plasma membrane, which is essential for normal development of *M. polymorpha*. In Chapter 3, I firstly observed the behavior of organelles during spermatid formation, because Mp*RAB23* was specifically expressed in the male reproductive organ, antheridiophores, and found that cell-autonomous degradative pathways are highly active

during spermiogenesis, which could be involved in removal of plasma membrane proteins and the cytoplasm. I then carried out analyses of MpRAB23, and found that MpRAB23 is essential for the proper organization of the microtubule-related structures in spermatozoids including the axoneme in flagella. These findings indicated that neofunctionalization and secondary loss of RAB GTPases played important roles in diversification and evolution of the membrane trafficking system during land plant evolution.
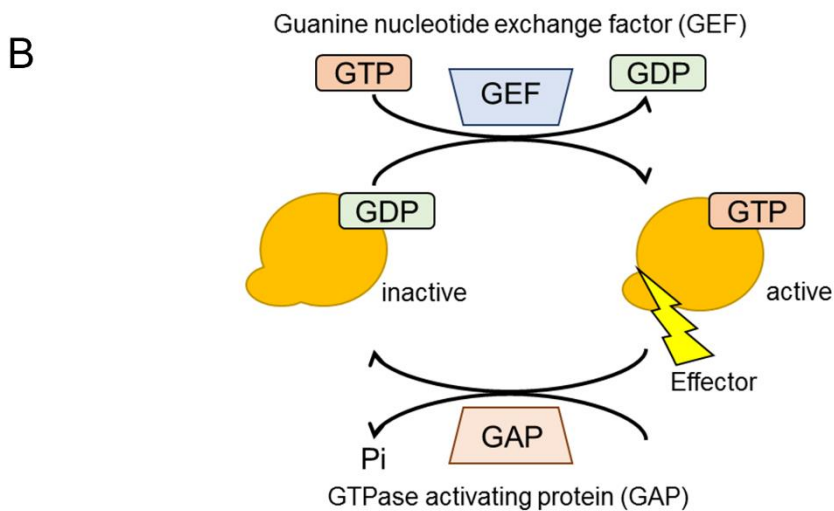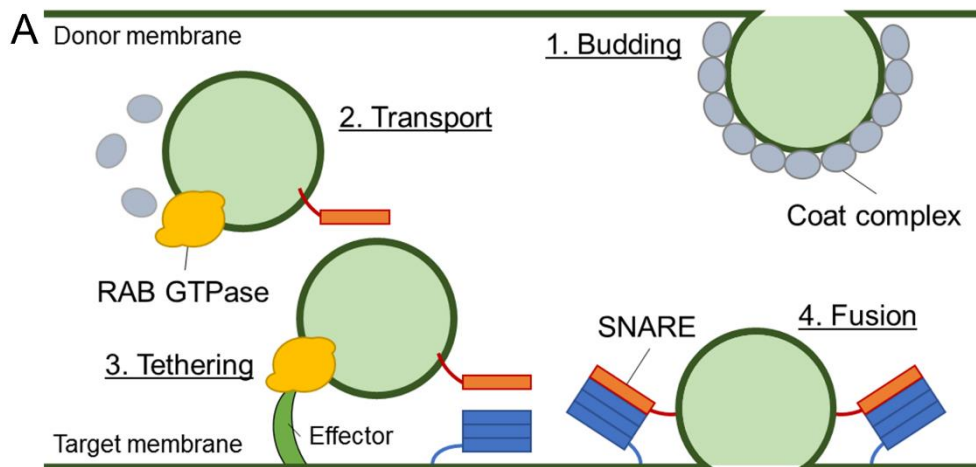
Figure 1. Framework of general mechanisms of membrane traffic

(A) A scheme of vesicle-mediated transport between organelles. Coat protein complexes mediate cargo selection and vesicle budding. RAB GTPase promotes tethering of the vesicle to the target membrane, which is mediated by effector proteins. Then SNARE proteins execute membrane fusion between the vesicle and target membrane. (B) RAB GTPase cycles between inactive GDP-bound and active GTP-bound forms. The guanine nucleotide exchange factor (GEF) and GTPase activating protein coordinate the GTPase cycle. Activated RAB GTPase interacts with specific effector molecules to evoke downstream events including vesicle tethering.
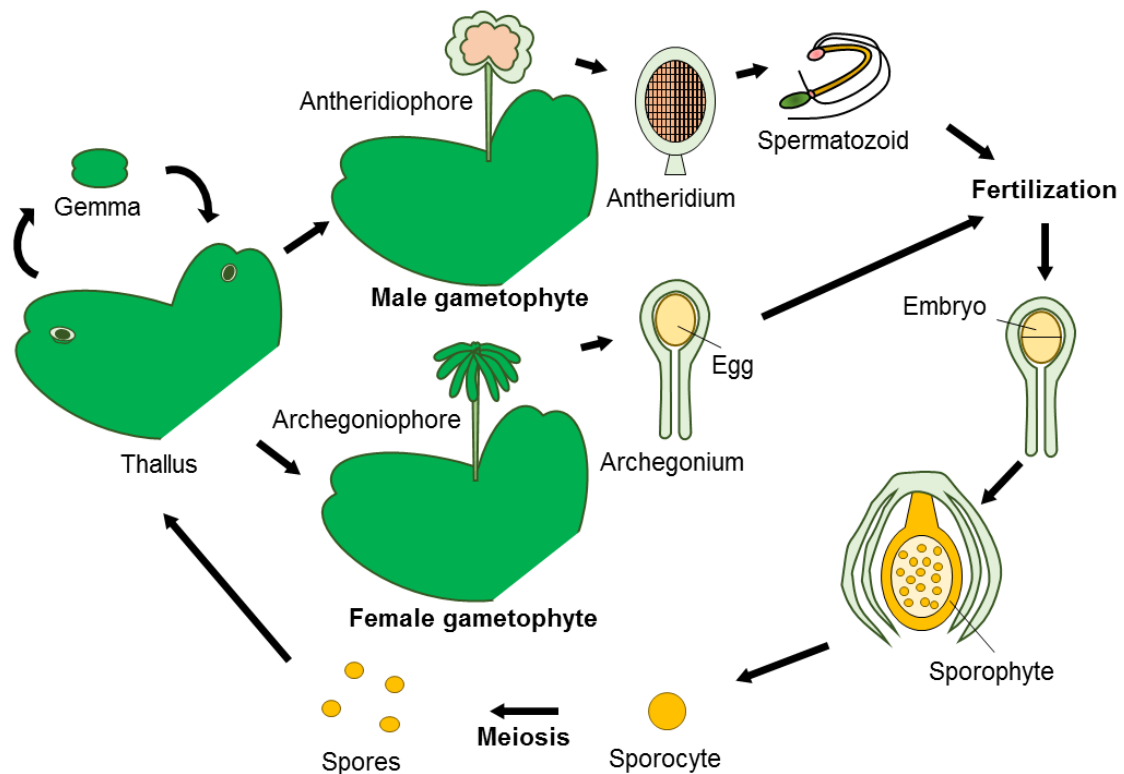
Figure 2. Life cycle of the liverwort, *M. polymorpha*

An overview of the life cycle of *M. polymorpha* is illustrated. In the life cycle of *M. polymorpha*, the haploid gametophyte generation is dominant. The thallus is a main plant body, and asexually reproduces through the formation of gemmae. *M. polymorpha* is a dioecious plant forming male and female reproductive organs (antheridiophores and archegoniophores) on different thalli. An antheridium and archegonium are male and female gametangia, respectively. Numerous motile gametes, spermatozoids are produced in antheridia, which swim to eggs in water to accomplish fertilization. After fertilization, a zygote develops into a sporophyte in the archegonium. After the sporophyte undergoes meiosis, numerous spores are formed in a capsule under the receptacle of the archegoniophore. A unicellular spore germinates and develops into the thallus.

Experimental procedures

Plant materials and Transformation

Male and female accessions of *M. polymorpha*, Takaragaike-1 (Tak-1) and Takaragaike-2 (Tak-2), respectively, were used in this study. These plants were grown on 1/2× Gamborg's B5 medium containing 1.4% (w/v) agar at 22°C under continuous white light. F1 spores generated by crossing Tak-1 and Tak-2 were used for transformation. Induction of sexual organs by far-red irradiation was performed as described previously (Chiyoda et al., 2008). Transgenic lines expressing Citrine-MpRAB5 and MpARA6-Venus were previously described (Era, 2012). Transgenic lines expressing ST-mRFP, mRFP-MpSYP6A or mCitrine-MpSYP2 were previously described (Kanazawa et al., 2016). Transgenic lines expressing sec-mRFP, mCitrine-MpVAMP71 or mCitrine-MpPIP2 were provided by Dr. Takehiko Kanazawa (Kanazawa 2016, and Kanazawa, unpublished).

Phylogenetic analysis and domain search

The genome databases used to collect amino acid sequences are described in Table 1. Collected amino acid sequences were aligned with the MUSCLE program version 3.8.31 (Edgar, 2004). After removing alignment gaps using Gblocks (http://molevol.cmima.csic.es/castresana/Gblocks_server.html), phylogenetic analysis was performed using PhyML 3.0 (http://www.atgc-montpellier.fr/phyml/) under the LG + G model which was selected by Smart Model Selection in PhyML. The bootstrap analysis was performed by resampling 1,000 sets. Prediction of the NLS and lipid modification sites was performed at NLS Mapper (http://nls-mapper.iab.keio.ac.jp/cgi-bin/NLS_Mapper_form.cgi) and GPS-lipid (http://lipid.biocuckoo.org/webserver.php), respectively. The genome and transcriptome databases used to examine the distribution

of *RAB21* and *RAB23* in green plants are described in Table 1.

RT-PCR

The primers used in this study and numbers of PCR cycles for the RT-PCR analysis are listed in Experimental procedures. RT-PCRs were performed using KOD FX neo (Toyobo) using cDNA prepared by Dr. Takehiko Kanazawa (Kanazawa et al., 2016) as templates according to the manufacturer's protocol.

Constructs and transformation

Open reading frames (ORFs) of RAB GTPases and Mp*VPS35* were amplified by PCR using cDNA prepared from Tak-1 or Tak-2 thalli or antheridiophores as templates. Amplified fragments were subcloned into the pENTR™/D-TOPO vector (Invitrogen). The fragments of RAB GTPases of *M. polymorpha* were introduced into pKI-GWB2, pKI-GWB3, pMpGWB302, pMpGWB305, or pMpGWB306 using the Gateway LR Clonase™ II Enzyme Mix (Invitrogen) according to the manufacturer's instructions. GTP-fixed or GDP-fixed type of Mp*RAB21* was constructed by PCR-mediated mutagenesis using the ORF of Mp*RAB21* subclomed in the pENTR™/D-TOPO vector. The GTP-fixed type of Mp*RAB21* was introduced into pMpGWB305 using the Gateway LR Clonase™ II Enzyme Mix.

To construct *mCitrine*-Mp*RAB5*, *mCitrine*-Mp*RAB21*, *mCitrine*-Mp*RAB23*, Mp*IFT52-mGFP*, Mp*TUG1-mGFP*, and Mp*KIN2-mGFP*, the genomic sequences comprising the 5' sequences (5.1 kb for Mp*RAB21*, 4.1 kb for Mp*RAB23*, 5.4 kb for Mp*IFT52*, 5.1 kb for Mp*TUG1*, and 5.3 kb for Mp*KIN2*), protein-coding regions (2.2 kb for Mp*RAB21*, 2.4 kb for Mp*RAB23*, 5.3 kb for Mp*IFT52*, 4.2 kb for Mp*TUG1*, and 6.5

kb for Mp*KIN2*), and 3' flanking sequences (2.2 kb for Mp*RAB21*, 1.4 kb for Mp*RAB23*, 2.5 kb for Mp*IFT52*, 2.2 kb for Mp*TUG1*, and 2.4 kb for Mp*KIN2*) were amplified by PCR and subcloned into the pENTR™/D-TOPO vector. The genomic sequence of Mp*RAB21* was mutated in the PAM sequence by PCR-mediated mutagenesis to generate the CRISPR-resistant construct. Each of DNAs for fluorescent proteins was then inserted in front of the start codon or in front of the stop codon using the In-Fusion HD Cloning System (Clontech) according to the manufacturer's instructions. The GTP-fixed type of MpRAB23 and MpRAB23 whose NLS-like sequence was mutated were constructed by PCR-directed mutagenesis. The chimeric genes were introduced into pMpGWB101 or pMpGWB301 (Ishizaki et al., 2015), using the Gateway LR Clonase™ II Enzyme Mix.

cDNAs for Mp*GOS11*, Mp*SYP6A*, and Mp*TUB2* were introduced into pMpGWB101 or pMpGWB301-based binary vectors containing *pro*Mp*SYP2:mCitrine*-Gateway (Minamino et al., 2017, and Kanazawa, unpublished). to obtain *pro*Mp*SYP2:mCitrine*-Mp*GOS11,* *pro*Mp*SYP2:mCitrine*-Mp*SYP6A,* and *pro*Mp*SYP2:mCitrine*-Mp*TUB2*.

The pENTR™/D-TOPO vectors containing Mp*SYP6A*, Mp*RAB5*, Mp*ARA6*, or Mp*RAB21*, and the constructs for expression of Citrine-MpRAB5 and MpARA6-Citrine under the regulation of the *cauliflower mosaic virus (CaMV) 35S* promoter were provided by Dr. Atsuko Era. The pENTR™/D-TOPO vectors containing Mp*RAB11a1*, Mp*RAB11a2* or Mp*RAB11b* were provided by Dr. Rin Asaoka. The pENTR™/D-TOPO vector containing Mp*TUB2* was provided by Dr. Ryuichi Nishihama. The pENTR™/D-TOPO vector containing Mp*GOS11*, the construct for expression of *sec-mRFP* under the regulation of the Mp*EF1α* promoter, and the constructs for expression of *mCitrine*-Mp*SYP12A*, *mCitrine*-Mp*SYP13A*, *mCitrine*-Mp*SYP2*, *mCitrine*-Mp*VAMP71*, and

mCitrine-Mp*PIP2* under the regulation of native promoters were provided by Dr. Takehiko Kanazawa (Kanazawa et al., 2016, Kanazawa, 2016, Kanazawa, unpublished).

To generate the construct for genome editing in the Mp*RAB21* gene, the sequence of guide RNA (gRNA) was inserted into the *Bsa*I site of pMpGE En03 (Sugano, unpublished) using the DNA ligation kit Ver.2.1 (Takara), and then introduced into the pMpGE010 binary vector (Sugano, unpublished) using the Gateway LR Clonase™ II Enzyme Mix (Invitrogen) according to the manufacturer's instructions.

To generate the construct for deletion of the Mp*RAB23* gene, the 3.7 kb Mp*RAB23* 5'-flanking sequence was amplified by PCR from genomic DNA, and inserted into the *Pac*I site of the pJHY-TMP1 vector (Ishizaki et al., 2013) using the In-Fusion HD Cloning System (Clontech) according to the manufacturer's instructions. Subsequently, the 3.6 kb Mp*RAB23* 3'-flanking sequence amplified by PCR was inserted into the *Asc*I site of the vector using the In-fusion System.

Transformation of *M. polymorpha* was performed according to the previously described method (Ishizaki et al., 2008; Kubota et al., 2013). Transgenic lines were selected with 10 mg l^{-1} hygromycin B and 100 mg l^{-1} cefotaxime for pKI-GWB2, pKI-GWB3, pMpGWB101, pMpGE010, and pJHY-TMP1, and 0.5 μM chlorsulfuron and 100 mg l^{-1} cefotaxime for pMpGWB301, pMpGWB302, pMpGWB303, pMpGWB305, and pMpGWB306.

Microscopy

Subcellular localizations of fluorescently tagged proteins in thallus cells were observed in 4~5-day-old gemmalings of transgenic *M. polymorpha* grown on the 1/2× Gamborg's B5 medium containing 1% (w/v) sucrose and 1.4% (w/v) agar at 22°C under continuous

white light under a confocal microscope (LSM780, Carl Zeiss) with an oil immersion lens (×63). To visualize endocytic compartments, thalli were soaked in 1 μM *N*-(3-Triethylammoniumpropyl)-4-(4-(Dibutylamino) Styryl) Pyridinium Dibromide (FM1-43, Thermo Scientific) diluted in distilled water and incubated for 30 min ~ 3 h at room temperature. Spectral unmixing and processing of obtained images were performed using the ZEN2012 software (Carl Zeiss). Samples were excited at 488 nm (Argon 488) and/or 561 nm (DPSS 561-10) and emitted fluorescence between 482 nm and 650 nm was recorded. To observe forming cell plates, thallus cells were observed under a BX51 microscope (Olympus) equipped with the confocal scanner unit CSU10 (Yokogawa Electric).

For imaging of antheridial cells of transgenic lines, the antheridial receptacles between stages 3 and 5 (Higo et al., 2016) were sliced manually with a razor blade, placed on a glass slide, and then covered with a cover slip. To observe the spermatids of the MpIFT52-mGFP expressing line, antheridia were fixed for 60 min with 4% (w/v) paraformaldehyde (PFA) in PME buffer (50 mM PIPES-KOH, 5 mM EGTA, and 1 mM MgSO₄, pH 7.0), and treated for 30 min with cell wall digestion buffer (1% (w/v) cellulase, 0.25% (w/v) pectolyase Y-23, 1% (w/v) BSA, 0.1% (w/v) IGEPAL CA-630, 1% glucose, and 1× cOmplete™ EDTA-free protease inhibitor cocktail (Roche Applied Science) in PME buffer). The samples were placed on a MAS-coated glass slide (Matsunami) and then covered with a cover slip. Antheridia and fixed spermatids were observed under a confocal microscope (LSM780, Carl Zeiss) with an oil immersion lens (×63).

For immunostaining, antheridia were fixed for 60 min with 4% (w/v) PFA in PME buffer and treated for 30 min with the cell wall digestion buffer. Cells were then treated with permeabilization buffer (0.1% (v/v) Triton X-100 and 1% (w/v) BSA in PME

buffer) for 10 min. After washing with PME buffer three times, cells were placed on a MAS-coated glass slide, and incubated for 60 min at room temperature with blocking solution (1% (w/v) BSA in PBS buffer). After removing blocking solution, cells were incubated with the monoclonal anti-acetylated tubulin antibody in PBS buffer at 4℃ overnight. After washing with PBS buffer three times, the samples were incubated for 60 min at 37℃ with the Alexa Fluor 405 goat anti-mouse IgG in PBS buffer. After washing with PBS buffer three times, slides were mounted using the ProLong Gold Antifade reagent (Thermo Fisher Scientific). Samples were observed under a confocal microscope (LSM780, Carl Zeiss) with an oil immersion lens (×63).

To trace movement of spermatozoids, spermatozoids were observed under a dark field microscope (Olympus) equipped with an ORCA-Flash4.0 V2 camera (Hamamatsu photonics).

The obtained images were processed with ImageJ (National Institute of Health) and Photoshop (Adobe Systems) softwares. The trajectories of spermatozoids were obtained by using the ImageJ macro, Color Footprint Rainbow.

Electron microscopy

Tak-1 antheridia at different stages were collected and fixed with 2% (w/v) PFA and 2% (w/v) glutaraldehyde in 0.05 M cacodylate buffer pH 7.4 at 4°C overnight. The fixed samples were washed 3 times with 0.05 M cacodylate buffer for 30 min each and were then post-fixed with 2% (w/v) osmium tetroxide in 0.05 M cacodylate buffer at 4°C for 3 h. The samples were dehydrated in graded ethanol solutions (50 and 70% (v/v) ethanol for 30 min each at 4°C, 90% (v/v) for 30 min at room temperature, 4 times of 100% (v/v) for 30 min each at room temperature, and 100% (v/v) overnight at room temperature).

The samples were infiltrated with propylene oxide (PO) two times for 30 min each, and then placed into a 70:30 mixture of PO and resin (Quetol-651; Nisshin EM Co.) for 1 h. The caps of tubes were opened overnight to volatilize PO. The samples were transferred to fresh 100% (v/v) resin and polymerized at 60°C for 48 h. Ultra-thin sample sections were mounted on copper grids, stained with 2% (w/v) uranyl acetate and lead stain solution (Sigma–Aldrich), and observed under a transmission electron microscope (JEM-1400Plus; JEOL Ltd) at an acceleration voltage of 80 kV. Digital images (2048 × 2048 pixels) were obtained using a CCD camera (VELETA; Olympus Soft Imaging Solutions GmbH).

Yeast Two-hybrid Assay

The cDNAs for wild-type and mutant versions of Mp*RAB21* were subcloned into pBD-GAL4-GWRFC. pBD-GAL4 vectors containing Mp*RAB5*, Mp*ARA6*, and Mp*RAB7*, and the pAD-GAL4 vector containing Mp*VPS9* were provided by Dr. Mariko Sunada (Sunada, 2015). Plasmids containing each of RAB GTPases and Mp*VPS9* were introduced into the AH109 strain (Clontech). Empty vectors were used for negative controls. At least three colonies were checked for interaction for each transformation.

Expression and purification of GST Fusion Proteins

GST-fused MpRAB21 was expressed in the *E. coli* Rosetta strain using the pGEX-6p-1 vector (GE Healthcare). Cells expressing GST fusion proteins were collected and resuspended in lysis buffer (50 mM Tris-HCl, pH7.5, 150 mM NaCl, 1% Triton X-100, 0.1% mercaptoethanol, and 1× cOmplete™ EDTA-free protease inhibitor cocktail (Roche Applied Science)), sonicated, and centrifuged at 10,000×*g* for 30 min. Supernatants were

mixed with glutathione-Sepharose 4B beads and incubated with rotation for 2 h at 4°C. The beads were washed with wash buffer (50 mM Tris-HCl, pH 7.5, 150 mM NaCl, and 1% Triton X-100), and then fusion proteins were eluted with elution buffer (50 mM Tris-HCl, pH 7.5, 150 mM NaCl, and 100 mM glutathione). The extracted protein was desalted with a PD-10 column (GE Healthcare). MpRAB5, MpRAB7, and MpVPS9, which were fused with GST, were provided by Dr. Mariko Sunada (Sunada, 2015).

Nucleotide-Exchange Assay

Nucleotide exchange on purified GST-tagged RAB GTPases was measured by monitoring the total fluorescent change of the fluorescent GDP analogue 2'-(or -3')-*O*-(*N*-Methylanthraniloyl)-GDP (Mant-GDP, Thermo Fisher Scientific). Each purified RAB GTPase was preloaded with Mant-GDP for 2 h and incubated with or without GST-MpVPS9 in reaction buffer (50 mM Tris-HCl, pH 8.0, 150 mM NaCl, and 0.5 mM $MgCl_2$) for 100 s at 25°C. Then, GMP-PNP was added to 0.1 mM to start the nucleotide-exchange reaction. The fluorescence change was detected with a fluorescence spectrophotometer (model F-2500; Hitachi High Technologies) at an excitation wavelength of 360 nm and an emission wavelength of 440 nm.

Antibodies

The antibody against Citrine was prepared by the purifying anti-GFP polyclonal antibody (Kanazawa et al., 2016) by affinity column chromatography. The antibodies against MpVPS9 was provided by Dr. Mariko Sunada (Sunada, 2015). The anti-GDI antibody was from the lab stock (Ebine et al., 2011). The polyclonal antibody against MpSYP2 was provided from Dr. Takehiko Kanazawa. The antibody against AtVPS35 was provided

by Dr. Ikuko Hara-Nishimura (Shimada et al., 2006). The monoclonal antibody against GFP (JL-8) was purchased from Clontech. The monoclonal antibody against acetylated tubulin was purchased from Sigma-Aldrich. The Alexa Fluor 405 goat anti-mouse IgG was purchased from Thermo Fisher Scientific. The dilution of each antibody in western blotting was as follows: anti-Citrine, 1:500; anti-MpVPS9, 1:500; anti-GDI, 1:1000; anti-MpSYP2, 1:500; anti-AtVPS35, 1:500; anti-GFP, 1:5000; anti-acetylated tubulin, 1:1000; and the Alexa Fluor 405 goat anti-mouse IgG, 1:1000.

Immunoprecipitation

7-day-old thalli grown on 1/2× Gamborg's B5 medium containing 1% (w/v) sucrose and 1.4% (w/v) agar were ground in immunoprecipitation buffer (50 mM HEPES-KOH, 400 mM sucrose, 5 mM $MgCl_2$, 1× cOmplete^{TM} EDTA-free protease inhibitor cocktail (Roche Applied Science), pH 7.5) and protein concentration was adjusted at 0.5 g l^{-1}. Lysates were centrifuged at 1,000×*g* for 10 min followed by centrifuging at 3,000×*g* for 10 min at 4°C to eliminate cell debris. Triton X-100 was then added to the supernatants to 1%, and the samples were rotated for 60 min at 4°C. The samples were centrifuged at 20,000×*g* for 30 min at 4°C, and the supernatants were subjected to co-immunopresipitation using the μMACS GFP Isolation Kit (Miltenyi Biotec), according to the manufacturer's instructions.

Preparation for Mass spectrometry (MS)

Immunoprecipitates obtained with the above method were separated by SDS-PAGE and stained with Flamingo Fliorescent Gel Stain (Bio-Rad). After lanes were cut from the gel, the gel-sliced samples were dehydrated with acetonitrile and dried in a vacuum desiccator.

The samples were deoxidized with 10 mM DTT in 25 mM NH_4HCO_3 for 1 h at 56 ℃. After washing with 25 mM NH_4HCO_3 for 10 min, the samples were alkylated with 55 mM iodoacetamide in 25 mM NH_4HCO_3 for 45 min at room temperature in the dark. After washing with 25 mM NH_4HCO_3 for 10 min, the samples were dehydrated with 50% (v/v) acetonitrile in 25 mM NH_4HCO_3 for 10 min twice, and then dried in a vacuum desiccator. After incubating with 10 μg/ml trypsin in 50 mM NH_4HCO_3 for 30 min on ice, excess solution was removed, and the samples were incubated overnight at 37 ℃. Digested peptides were extracted with 50% (v/v) acetonitrile and 5% (v/v) trifluoroacetic acid for 30 min at room temperature, and then extraction was repeated with new solution. The peptides were dissolved in 30% (v/v) acetonitrile and 0.1% (v/v) formic acid and then analyzed with Orbitrap Elite (Thermo Fisher Scientific) using Mascot ver.2.5.1 (Matrix science, London W1U 7GB, UK).

Fractionation

7-day-old thalli grown on 1/2 Gamborg's B5 medium containing 1% (w/v) sucrose and 1.4% (w/v) agar were ground in grinding buffer (50 mM HEPES-KOH, 250 mM sorbitol, 2mM EGTA, and 5 mM $MgCl_2$, pH 7.5) and adjusted to the protein concentration at 0.5 g l^{-1}. Lysates were centrifuged at 1,000×g for 10 min followed by centrifuging at 3,000×g for 10 min at 4℃ to eliminate cell debris. The total cell lysate (T) was centrifuged at 100,000×g for 1 h at 4℃ to obtain soluble cytosolic (S) and pelleted membrane (P) fractions.

Expression of MpVPS35 in yeast

The ORF of Mp*VPS35* was inserted into the *Bgl*II site of pTU1containing the constitutive

TDH3 promoter (Ueda et al., 2001). YPH500 cells expressing MpVPS35 under the control of *TDH3* promoter were cultured in SD -Ura for 2 days, and were collected by centrifuging at 10,000×*g* for 1 min. Yeast cells were resuspended in 0.1 N NaOH, incubated for 15 min on ice, and then centrifuged at 10,000×*g* for 1 min (Kushnirov, 2000). Yeast cells were resuspended in sample buffer (65 mM Tris-HCl (pH6.8), 3% (w/v) SDS and 10% (v/v) glycerol), boiled for 5 min, and then centrifuged at 10,000×*g* for 1 min to eliminate the cell debris to apply to immunoblotting.

Tables

Table 1. A list of genome and transcriptome datasets used in this study

Deposited Data	Source	Identifier
Arabidopsis thaliana genome TAIR10	Phytozome	https://phytozome.jgi.doe.gov/pz/portal.html#
Nicotiana tabacum genome	NCBI	https://www.ncbi.nlm.nih.gov/
Nelumbo nucifera genome	Ming et al., 2013	https://www.ncbi.nlm.nih.gov/
Brachypodium distachyon genome	Phytozome (International Brachypodium, 2010)	https://phytozome.jgi.doe.gov/pz/portal.html#
Zea mays genome	Phytozome (Schnable et al., 2009)	https://phytozome.jgi.doe.gov/pz/portal.html#
Oryza sativa genome	RAP DB (Sakai et al., 2013, Kawahata et al., 2013)	http://rapdb.dna.affrc.go.jp/
Amborella trichopoda genome v1.0	Amborella Genome, 2013	http://amborella.huck.psu.edu/home
Ginkgo biloba genome	Guan et al., 2016	http://gigadb.org/dataset/100209
Selaginella moellendorffii genome v1.0	Phytozome (Banks et al., 2011)	https://phytozome.jgi.doe.gov/pz/portal.html#
Marchantia polymorpha genome v3.1	MarpolBase (Bowman et al., 2017)	http://marchantia.info/
Physcomitrella patens genome v3.0	Phytozome (Rensing et al., 2008)	https://phytozome.jgi.doe.gov/pz/portal.html#
Spirogyra pratensis transcriptome	Ju et al., 2015	https://www.ncbi.nlm.nih.gov/ Traces/wgs/?val=GBSM01
Coleochate orbicularis transcriptome	Ju et al., 2015	https://www.ncbi.nlm.nih.gov/ Traces/wgs/?val=GBSL01
Nitella mirabilis transcriptome	Ju et al., 2015	https://www.ncbi.nlm.nih.gov/ Traces/wgs/?val=GBST01
Klebsormidium nitens genome	Hori et al., 2014; Ohtaka et al., 2017	http://www.plantmorphogenesis.bio.titech.ac.jp/ ~algae_genome_project/klebsormidium/ kf_download.htm
Mesostigma viride transcriptome	Ju et al., 2015	https://www.ncbi.nlm.nih.gov/ Traces/wgs/?val=GBSK01
Chlamydomonas reinhardtii genome	Phytozome (Merchant et al., 2007)	https://phytozome.jgi.doe.gov/pz/portal.html#
Coccomyxa subellipsoidea genome	Phytozome (Blanc et al., 2012)	https://phytozome.jgi.doe.gov/pz/portal.html#
Ostreococcus tauri genome	Derelle er al., 2006	https://bioinformatics.psb.ugent.be/gdb/ ostreococcus/
Homo sapiens genome	NCBI	https://www.ncbi.nlm.nih.gov/

Table 2. A list of MpRAB members and their gene IDs

name	geneID
Mp*RAB1a*	Mapoly0072s0030.1
Mp*RAB1b*	Mapoly0007s0067.1
Mp*RAB2a*	Mapoly0170s0032.1
Mp*RAB2b*	Mapoly0100s0038.1
Mp*RAB5*	Mapoly0036s0134.1
Mp*ARA6*	Mapoly0077s0027.1
Mp*RAB6*	Mapoly0141s0004.1
Mp*RAB7*	Mapoly0946s0001.1
Mp*RAB8a*	Mapoly0116s0012.1
Mp*RAB8b*	Mapoly0057s0033.1
Mp*RAB8c*	Mapoly0015s0029.1
Mp*RAB11a1*	MapolyY_A0041.1
Mp*RAB11a2*	Mapoly0018s0008.1
Mp*RAB11b*	Mapoly0050s0009.1
Mp*RAB11c*	Mapoly0007s0069.1
Mp*RAB18*	Mapoly0167s0019.1
Mp*RAB21*	Mapoly0001s0443.1
Mp*RAB23*	Mapoly0020s0116.1

Table 3. A list of primers used in this study

Purpose	Frangment	primer 1 (5' to 3')	primer 2 (5' to 3')	PCR cycles
Plasmid construction for ORF sequences	MpRAB1a	CACCATGAATCCCGAGTATGATTACC	TCATGTGCAACAGCCTTGCTTTTG	
	MpRAB1b	CACCATGAACCCCGAATATGATTATC	TCAGGAGCAACACCCACCGCTCTG	
	MpRAB2a	CACCATGTCTTACGCGTACCTCTTC	TCAACCACAGCAACCACCTTTGG	
	MpRAB2b	CACCATGCCTTCGACATCGCCGTC	CTAAATCCCGCACTTCAACA	
	MpRAB5	CACCATGGCCACCGCGGGAACGAA	CTAGACGCAGCACATGCTTG	
	MpARA6	CACCATGGGTTGTGCTGCCTCAGC	AGGCTTCTGGGTTGGCTGT	
	MpRAB6	CACCATGGCGTCAGCAGGAATGGGGAC	TTAGCAGGCGCAGCCCCCGCT	
	MpRAB7	CACCATGTCAGCTCGTAAACGAAC	TCAGCATTCACAGACAGATG	
	MpRAB8a	CACCATGGCAGCAGGAGCAGCGAGAGC	CTAACTGCAGCAAGCTGATTTTTG	
	MpRAB8b	CACCATGGCGGACAGTGATTACCGCATG	TCACCCGCAGCAGTTTTGGTAATTG	
	MpRAB8c	CACCATGGGGAACCCGGACTATTGC	TTACGAGGCACCGCAGCAGCCAG	
	MpRAB11a	CACCATGGCTTATAGATCCGACGATG	TTACGCTGAGCAACATCCTAC	
	MpRAB11b	CACCATGATGTCAAACGGATATGGAG	CTAAGTTGAACAGCAAGCTTTC	
	MpRAB11c	CACCATGGGGTACGGTGACGATGAGAAG	TTAACAGCAGCCAAATCTCTTTG	
	MpRAB18	CACCATGGCCGGGGGCAGTGGTGC	TCAACATGTACAGTTACCAGC	
	MpRAB21	CACCATGAGGCCTGGCCCGACATT	TCAAGAACAACACTTCGAAG	

24

	MpRAB23	CACCATGCTGTCGA TGCAGGAAGAAG	CTACAAAATTGAAC ACTCGGACTGC	
	MpVPS35	CACCATGCAGCCTC AAGGCGAGGTG	CTATATTTGTATTGC GGCATATCG	
RT-PCR	MpRAB1a	CACCATGAATCCCG AGTATGATTACC	TCATGTGCAACAGC CTTGCTTTTG	30
	MpRAB1b	CACCATGAACCCCG AATATGATTATC	TCAGGAGCAACACC CACCGCTCTG	29
	MpRAB2a	CACCATGTCTTACG CGTACCTCTTC	TCAACCACAGCAAC CACCTTTGG	31
	MpRAB2b	ATGCCTTCGACATC GCCGTCAATGC	CTAAATCCCGCACT TCAACACCTCC	34
	MpRAB5	CACCATGGCCACCG CGGGAACGAA	CTAGACGCAGCACA TGCTTG	28
	MpARA6	CACCATGGGTTGTG CTGCCTCAGC	AGGCTTCTGGGTTG GCTGTC	30
	MpRAB6	CACCATGGCGTCAG CAGGAATGGGGAC	TTAGCAGGCGCAGC CCCCCGCT	30
	MpRAB7	CACCATGTCAGCTC GTAAACGAAC	TCAGCATTCACAGA CAGATG	29
	MpRAB8a	CACCATGGCAGCAG GAGCAGCGAGAGC	CTAACTGCAGCAAG CTGATTTTTG	30
	MpRAB8b	CACCATGGCGGACA GTGATTACCGCATG	TCACCCGCAGCAGT TTTGGTAATTG	31
	MpRAB8c	CACCATGGGGAACC CGGACTATTGC	TTACGAGGCACCGC AGCAGCCAG	33
	MpRAB11a	CACCATGGCTTATA GATCCGACGATG	TTACGCTGAGCAAC ATCCTAC	28
	MpRAB11b	CACCATGATGTCAA ACGGATATGGAG	CTAAGTTGAACAGC AAGCTTTC	32
	MpRAB11c	CACCATGGGGTACG GTGACGATGAGAAG	TTAACAGCAGCCAA ATCTCTTTG	30
	MpRAB18	CACCATGGCCGGGG GCAGTGGTGC	TCAACATGTACAGT TACCAGC	32
	MpRAB21	CACCATGAGGCCTG GCCCGACATT	TCAAGAACAACACT TCGAAG	34

	MpRAB23	ATGCTGTCGATGCAGGAAGAAGACTTC	CTACAAAATTGAACACTCGGACTGCAATC	38
	mCitrine-MpRAB23	ATGGTGAGCAAGGGCGAGGA	CTACAAAATTGAACACTCGGACTGCAATC	
	MpEF1a	TCACTCTGGGTGTGAAGCAGATGA	GCCTCGAGTAAAGCTTCGTGGTG	24
Plasmid construction for genomic sequences	MpRAB5 promoter + 5' UTR	GCAGGCTCCGCGGCCGCATTAAGGCATGATATTGAAGATAAG	GTGAAGGGGGCGGCCCCTCGCTACCCTTCAATCACACGCT	
	MpRAB5 protein coding region +3' flanking sequence	CCAAGGGTGGGCGCGGCATGGCCACCGCGGGAACGAATCAG	AGCTGGGTCGGCGCGGAATGTGACTGAACTCCGTCAGC	
	MpRAB5 fragment for mCitrine insertion	GCCCTTGCTCACCATCCTCGCTACCCTTCAATCAC	AAGGGAGGATGCGGAATGGCCACCGCGGGAACGAATC	
	MpRAB21 promoter + 5' UTR	AAAAGCAGGCTCCGCTGGAACTAGAGAATGTGGTCGCTC	GTGAAGGGGGCGGCCGCTGCCCCGCCCAAAGAAATCG	
	MpRAB21 protein coding region +3' flanking sequence	CACCCCCGGGGGAAGCGGAATGAGGCCTGGCCCGACATTTAAG	CTGTTAGCTTGTGAGCTATTGCCAG	
	MpRAB23 genomic region	CACCGCAAGCTGTCCTCGTCTCAACAAC	CCTTCAGACCAGCAAGTATACAC	
	MpRAB23 fragment for mCitrine insertion	AAGGGAGGATGCGGAATGCTGTCGATGCAGGAAGAAGAC	GCCCTTGCTCACCATGATGTCACCGCTTAG CGCACTC	
	MpIFT52	CACCGGTTAACATC	CTTGAGGAACGCGA	

genomic region	CGATAGATTTGTGGAAG	AGACTTCTCC	
MpIFT52 fragment for mGFP insertion	GACGAGCTGTACAAGTAGGTTTATGACCTGACCGG	CACTCCGCTTCCTCCCTCCTCAATATTTTCCGAATGAC	
MpTUG1 genomic region	CACCATGTAGAATGAAATCATGGTCACTG	CGGTACAGACAACTAATCGCAGTC	
MpTUG1 fragment for mGFP insertion	GACGAGCTGTACAAGTAGATTTTCCGGAAGCTGCGC	CACTCCGCTTCCTCCCAGAAGGGGCGCTCTTGAATC	
MpKIN2 promoter + 5' UTR	AAAAGCAGGCTCCGCCTTGTCTCTACATTGAAGTCACTGG	GTGAAGGGGGCGGCCTATTTCTCTTTATTCGATGAAAACTTG	
MpKIN2 protein coding region +3' flanking sequence	CACCATGTCGAAGATCATGAAAGAAAC	CACTATGTTCACATAATCCAGTGG	
MpKIN1 fragment for mGFP insertion-1	ACGAAACTGAAGTTGGATCCTTCAGCAC	CACTCCGCTTCCTCCTCTTGTTGCAGTTTTTGGGC	
MpKIN1 fragment for mGFP insertion-2	GACGAGCTGTACAAGTAACAAAATAAAATCAGTTGTCTGG	AGCTGGGTCGGCGCGCCCACCCTTCACTATG	
mCitrine + linker	ATGGTGAGCAAGGGCGAGGA	TCCGCATCCTCCCTTGTACAGCTCGTCCATGC	
linker + mGFP	GGAGGAAGCGGAGTGAGCAAGGGCGAGGAGC	CTTGTACAGCTCGTCCATGC	

Plasmid construction for generation of mutants	MpRAB21gRNA	CTCGAATAGATCGGCCCGAGTGCA	AAACTGCACTCGGGCCGATCTATT	
	Insertion for MpRAB23 gene targeting at *Pac* I site	CTAAGGTAGCGATTAATGAACGTCGTTACGGAGCTGTGCTTG	CCGGGCAAGCTTTTAATCATTTCCAACCACAACAACTTTCAC	
	Insertion for MpRAB23 gene targeting at *Asc* I site	TAAACTAGTGGCGCGCCTGCGAAGTTTCGCTCGGAATTTCA	TAAACTAGTGGCGCGCCTGCGAAGTTTCGCTCGGAATTTCA	
	CRISPR-resistant mutation for MpRAB21	AGGAACGCTTTCATGCACTC	CATGAAAGCGTTCCTGACCTG	
	GTP-fixed mutation for MpRAB21	CACTGCAGGTCTGGAACGCTTCC	GGAAGCGTTCCAGACCTGCAGTG	
	GDP-fixed mutation for MpRAB21	GCGTCGGGAAAAACTCTATGGTGTTACG	CGTAACACCATAGAGTTTTTCCCGACGC	
	GTP-fixed mutation for MpRAB23 genomic region-1	GGAGCACTTCCATCTCGAGACG	CTGCTCCAGCCCTGCAGTATC	
	GTP-fixed mutation for MpRAB23 genomic region-2	GCAGGGCTGGAGCAGTTTCATG	GGTGTCGAATGGATCCGTTATTG	
	MpRAB23 222-229 Ala genomic region-1	CAGCAATAACGGATCCATTCGAC	AGCGGCTGCGGCGGCGATGTTGATGACTTTCGATC	
	MpRAB23	GCCGCCGCAGCCGC	ACAAGAAGTTGAC	

	222-229 Ala genomic region-2	TGCAGCCTTGCAGTCCGAGTGTTCAATTTTG	GTCGAACTTG	
Others	a-b fragment of MpRAB23genotyping	CGAAGTCGAATGCGGTTGAGCA	CCAGACCTGAGGCAAGAACAGTC	
	c-d fragment of MpRAB23genotyping	GTATAATGTATGCTATACGAAGTTATGTTT	CTACCATGCATAAGCATATAACTC	
	MpRAB21 for pGEX6p-1	GGGCCCCTGGGATCCATGAGGCCTGGCCCG	GAATTCCGGGGATCCTCAAGAACAACACTTCG	
	*Bgl*I site + MpVPS35	GGCAGATCTATGCAGCCTCAAGGCGAGGTG	GGCAGATCTCTATATTTGTATTGCGGCATATCG	

29

Chapter 1

Characterization of RAB GTPases in *M. polymorpha*

Introduction

The composition of RAB GTPases in the plant lineage has distinctive characteristics. For example, the RAB11 group (also known as the RABA group in Arabidopsis) has dramatically expanded compared to other organisms; 26 members of RAB11 are encoded in the Arabidopsis genome, whereas only two or three RAB11 members exist in budding yeast and mammalian species (Rutherford and Moore, 2002). Diversified RAB11/RABA members in angiosperms have been shown to be involved in various biological functions specific to plants, such as salinity stress tolerance, elongation of root hairs and pollen tubes, cell plate formation, and polar cell expansion (Asaoka et al., 2013; Chow et al., 2008; de Graaf et al., 2005; Kirchhelle et al., 2016; Preuss et al., 2004). The RAB5 group (also known as RABF in Arabidopsis) represents another example of plant-unique diversification of RAB GTPases; in addition to canonical RAB5, the green plant lineage harbors a plant-unique RAB5 group, the ARA6 group. For example, Arabidopsis harbors two canonical RAB5 members, RHA1/RABF2a and ARA7/RABF2b, and the plant-specific ARA6/RABF1 (Ueda et al., 2001). Canonical RAB5 mediates endosomal transport in endocytic and vacuolar transport pathways in plant cells, whereas ARA6 acts in the trafficking pathway from endosomes to the plasma membrane (Ebine et al., 2011; Kotzer et al., 2004; Sohn et al., 2003). It was also recently shown that a function of canonical RAB5 is fulfilled through interaction with a plant-specific effector molecule (Sakurai et al., 2016), highlighting plant-specific methods of regulating endosomal transport. Thus, diversification of RAB GTPases in plants should be closely related to diversification of membrane trafficking systems during plant evolution.

Comparative genomics proposed that expansion of RAB GTPases in the plant lineage could be associated with terrestrialization and multicellularization, mainly based

on the increased number of RAB GTPases in land plants, including Arabidopsis and the moss *Physcomitrella patens* compared to that of green algal species (Dacks and Field, 2007; Rutherford and Moore, 2002). However, *P. patens* has been shown to undergo whole genome duplication during evolution (Rensing et al., 2007; Rensing et al., 2008), which could result in the increased number of RAB GTPases without functional differentiation or neofunctionalization. To precisely understand the relevance between diversification of the membrane trafficking component and plant evolution, information about other basal plant lineages would be useful.

The liverwort, *M. polymorpha* is an emerging model plant whose genome was sequenced recently (Bowman et al., 2017) and for which various molecular genetical and cell biological techniques are applicable (Chiyoda et al., 2008; Ishizaki et al., 2008; Ishizaki et al., 2013; Ishizaki et al., 2015; Kanazawa et al., 2016; Kubota et al., 2013; Nishihama et al., 2016; Sugano et al., 2014). For information on the organization of RAB GTPases in this plant, I sought genes encoding RAB GTPases in the genome of *M. polymorpha*. I then examined the expression pattern and subcellular localization of all members of RAB GTPases in this plant. My results revealed that *M. polymorpha* harbors a fundamental set of RAB GTPases shared with other green plant lineages with low redundancy. Furthermore, I found that *M. polymorpha* harbors RAB GTPases that were secondarily lost in Arabidopsis. *M. polymorpha* also harbors a RAB-like protein containing an intraflagellar transport protein-like domain. The unique repertoire of RAB GTPases suggests that the unique membrane trafficking system of *M. polymorpha* developed during its evolution to fulfill conserved and specific biological roles in the plant.

Results

The *M. polymorpha* genome encodes 17 predicted RAB GTPases

To gain insight into the diversification of membrane trafficking pathways during land plant evolution, I searched the genome database of *M. polymorpha* for genes predicted to encode RAB GTPases. I identified 17 genes for putative RAB GTPases, which were classified into 10 subgroups as follows: RAB1/RABD, RAB2/RABB, RAB5/RABF, RAB6/RABH, RAB7/RABG RAB8/RABE, RAB11/RABA, RAB18/RABC, RAB21, and RAB23 (Figure 3, 4 and Bowman et al., 2017). The names and gene IDs in MarpolBase (marchantia.info) of these members are listed in Table 2. I detected highly similar sequences for *RAB11a/RABA1* with two nonsynonymous and several synonymous substitutions. *M. polymorpha* is dioecious, and male and female plants harbor the X and Y chromosome, respectively (Bischler, 1986). Each of the *RAB11a* genes was mapped on the X or Y chromosome (Bowman et al., 2017); thus, I concluded that these two *RAB11a* genes are allelic and that male and female *M. polymorpha* plants harbor different alleles of *RAB11a* with slight variation (Figure 5).

Eight subgroups of RAB GTPases, RAB1/RABD, RAB2/RABB, RAB5/RABF, RAB6/RABH, RAB7/RABG, RAB8/RABE, RAB11/RABA, and RAB18/RABC, are well conserved in green plant lineages, and *M. polymorpha* possessed all of these subgroups with low redundancy (Figure 3, and Bowman et al., 2017). *M. polymorpha* possesses genes for *RAB21* and *RAB23*, which have not been identified in genomes of Arabidopsis. The *RAB21* and *RAB23* genes are found in a wide range of eukaryotic lineages, including metazoa, suggesting an ancestral origin for these RAB subgroups, whereas these RAB GTPases were independently secondarily lost several times during green plant evolution (Figure 6, and (Klopper et al., 2012). Notably, the distribution of

RAB23 gene is closely associated with the presence of a motile flagellum (Figure 6). A uniquely acquired RAB-like gene was also identified in *M. polymorpha*. The protein that I named MpRAB2b is larger than other RAB GTPases and contains a domain at the C-terminal region with high similarity to the INTRAFLAGELLAR TRANSPORT 43 (IFT43) protein (Figure 7). The conserved motifs responsible for nucleotide binding and the GTPase activity conserved in the Ras-superfamily are largely conserved in MpRAB2b, and a lipid modification site was also predicted at the C-terminus (Figure 7). IFT43 is a subunit of the IFT-A complex, which regulates retrograde transport in intra-flagellar transport (IFT) (Taschner et al., 2012). This type of RAB-like protein has not been reported in any other organisms, suggesting that this is a specific innovation of liverworts.

Expression patterns of *M. polymorpha* RAB GTPases

I examined the expression profiles of *M. polymorpha* RAB GTPases in several organs (5-day-old thalli, antheridiophores, archegoniophores, and 7-day-old sporelings) using reverse transcription (RT)-PCR, with constitutive Mp*EF1α* as a positive control (Althoff et al., 2014; Kanazawa et al., 2013). All *M. polymorpha* RAB genes were ubiquitously transcribed in these organs under our experimental conditions, with the exception of Mp*RAB2b* and Mp*RAB23* (Figure 8). Mp*RAB2b* and Mp*RAB23* transcripts were strongly accumulated only in the antheridiophores and were scarcely detected in the other organs (Figure 8) as previously described (Higo et al., 2016), suggesting specialized functions of MpRAB2b and MpRAB23 in the antheridiophores.

Subcellular localization of RAB GTPases in *M. polymorpha*

Subcellular localization is essential information for elucidating the functions of RAB

GTPases. To determine the subcellular localization of *M. polymorpha* RAB GTPases, I expressed Citrine (a variant of yellow fluorescent proteins)-fused RAB GTPases under the regulation of the *cauliflower mosaic virus (CaMV) 35S* promoter in thallus cells of *M. polymorpha*. As organelle markers, I utilized the transmembrane domain of rat sialyltransferase-fused monomeric red fluorescent protein (ST-mRFP) and mRFP-MpSYP6A, which are the Golgi apparatus and trans-Golgi network (TGN) markers, respectively (Kanazawa et al., 2016). For endosomal localization, I employed a lipophilic fluorescent dye, FM1-43, which stains endosomal compartments during endocytosis toward vacuoles. Based on colocalization with these markers and the tracer, I classified the subcellular localizations of *M. polymorpha* RAB GTPases into four groups.

Secretory RAB GTPases

Three RAB GTPases, MpRAB2a, MpRAB8a, and MpRAB8b exhibited punctate localization in thallus cells of *M. polymorpha* and colocalized with the Golgi apparatus marker ST-mRFP (Figure 9A, 9C, and 9E). The punctate structures were frequently and closely associated but not co-localized with the TGN marker mRFP-MpSYP6A (Figure 9B, 9D, and 9F). Citrine-MpRAB8c driven by the *CaMV 35S* promoter was dispersed into the cytosol, with punctate localization partly colocalized with ST-mRFP but not with mRFP-MpSYP6A (Figure 9G and 9H).

The subcellular localization of MpRAB1a, MpRAB1b, and MpRAB6 was slightly different from those of Golgi-localized RAB GTPases. These proteins were localized to disc-shaped compartments and smaller punctate structures that were frequently associated with the disc-shaped compartments. The disc-shaped compartments also bore ST-mRFP, and the punctate structures exhibited colocalization with mRFP-

MpSYP6A (Figure 10A-10F). This result indicates that MpRAB1a, MpRAB1b, and MpRAB6 localize at the Golgi apparatus and the TGN in thallus cells.

The MpRAB11/RABA group localizes to the TGN and TGN-associated compartments

There are three RAB11 genes in *M. polymorpha* that are classified with the RABA1, RABA4, and RABA5 subclasses of Arabidopsis (Figure 3, 4, and Bowman et al., 2017). Citrine fusion of these RAB11 members, MpRAB11a1 (the male allele), MpRAB11b, and MpRAB11c, driven by the *CaMV 35S* promoter localized to punctate compartments with variations in their sizes in thallus cells. All three RAB11 members were partly co-localized or closely associated with the TGN marker mRFP-MpSYP6A (Figure 11B, 11E, and 11H). Intriguingly, however, these RAB11 members exhibited distinct localizations in relation to the Golgi apparatus marker ST-mRFP; Citrine-MpRAB11c was co-localized with ST-mRFP (Figure 11G), but Citrine-MpRAB11a1 and Citrine-MpRAB11b were not (Figure 11A and 11D). A subpopulation of Citrine-MpRAB11a1-, 11b-, and 11c-positive compartments were accessible by FM1-43 (Figure 11C, 11F, and 11I), suggesting the endosomal identity of these compartments.

Some RAB11/RABA members in Arabidopsis have been localized to the forming cell plate and are involved in cell plate formation (Asaoka et al., 2013; Chow et al., 2008; Qi and Zheng, 2013). When I observed the meristematic zones of thalli, accumulation at forming cell plates was also observed for all of three RAB11 members in *M. polymorpha* (Figure 11J). This localization suggests that MpRAB11 members could also be involved in cell plate formation.

Endocytic/vacuolar RAB GTPases

The existence of two types of RAB5 is a distinctive feature of RAB GTPases in green plants. In addition, in *M. polymorpha*, the canonical MpRAB5 and plant-unique MpARA6 were identified, whose fluorescent protein-tagged versions were localized to endosomal punctate compartments stained by FM1-43 (Figure 12A and 12D). These proteins were not colocalized with ST-mRFP nor mRFP-MpSYP6A (Figure 12B, 12C, 12E, and 12F), whereas some MpRAB5-positive domains were observed in close vicinity to the MpSYP6A-positive TGN. When MpRAB5 driven by the *CaMV 35S* promoter and MpARA6 driven by the *MpEF1α* promoter were coexpressed in thalli tagged with different fluorescent proteins, only partial colocalization was observed (Figure 12G), as shown for RAB5/RABF2 and ARA6/RABF1 in Arabidopsis (Ebine et al., 2011; Ueda et al., 2004). The previous study demonstrated that these proteins are localized to multivesicular endosomes (MVEs) in thallus cells (Era, 2012), therefore MpRAB5 and MpARA6 reside on distinct population of MVEs with partial overlap as orthologous products in Arabidopsis.

The other three RAB GTPases, MpRAB7, MpRAB18, and MpRAB21, were also localized to endocytic organelles. Citrine-fused MpRAB7 driven by the *CaMV 35S* promoter was localized on the vacuolar membrane and punctate compartments in thallus cells. A portion of the punctate compartments were stained with FM1-43, whereas the other MpRAB7-positive compartments remained unstained (Figure 13A). The unstained structures likely represent Golgi apparatuses because ST-mRFP but not mRFP-MpSYP6A was colocalized with Citrine-MpRAB7 (Figure 13B and 13C). These results suggest that MpRAB7 was localized at the Golgi apparatus, endosomal compartments (probably the late endosome/MVE), and the vacuolar membrane.

Citrine-fused MpRAB18 driven by the *CaMV 35S* promoter was localized to punctate compartments, which were stained with FM1-43 (Figure 13D). MpRAB18 did not show colocalization with ST-mRFP or mRFP-MpSYP6A (Figure 13E and 13F), suggesting that MpRAB18 localizes on endosomal compartments in *M. polymorpha* thallus cells.

Citrine-fused MpRAB21 expressed under the control of the *CaMV 35S* promoter was localized at punctate structures accessible by FM1-43 (Figure 13G), which did not bear ST-mRFP or mRFP-MpSYP6A (Figure 13H and 13I), although MpRAB21-positive domains were sometimes observed to be closely associated with the MpSYP6A-positive TGN, similar to the localization pattern of MpRAB5.

Antheridiophore-specific RAB GTPases ectopically expressed in thalli

I also generated transgenic lines expressing Citrine-tagged MpRAB2b and MpRAB23 under the regulation of the *CaMV 35S* promoter, although expression of the genes for these proteins was only detected in antheridiophores by RT-PCR (Figure 8). Citrine-MpRAB2b was observed dispersed in the cytosol in thallus cells (Figure 14A), and Citrine-MpRAB23 accumulated in the nuclei of the thallus cells (Figure 14B). I found that MpRAB23 contained a nuclear localization sequence (NLS)-like domain rich in arginine and lysine residues near the C-terminus (Figure 15), because of which MpRAB23 could be localized in the nuclei of the thalli.

Discussion

In this study, I identified 17 genes for RAB GTPases in the genome of *M. polymorpha*. I demonstrated that *M. polymorpha* harbors fundamental sets of RAB GTPases, which are

conserved in other plant lineages with low redundancy. Previous studies proposed that expansion of genes for membrane trafficking components could be associated with adaptation to land and/or multicellularization of an ancestor of land plants (Rutherford and Moore, 2002; Sanderfoot, 2007). My results partly support this idea: the number of RAB GTPases in *M. polymorpha* is greater than that of unicellular algal species, and 10 and 9 RAB GTPases are encoded in the genomes of *Chlamydomonas reinhardtii* and *Ostreococcus tauri*, respectively. However, the number of RAB GTPases in Arabidopsis is much greater than that in *M. polymorpha*, which suggests that the expansion of RAB GTPases is not simply associated with terrestrialization and/or multicellularization. A similar result was also obtained in the systematic analysis of soluble *N*-ethylmaleimide-sensitive factor attachment protein receptor (SNARE) proteins in *M. polymorpha* (Kanazawa et al., 2016). It will be interesting to investigate what physiology and functions of land plants were associated with the diversification, specialization, or neofunctionalization of RAB GTPases during their evolution.

Conserved and Unique features of RAB GTPases in *M. polymorpha*

I examined the subcellular localizations of all RAB GTPases by fusion with florescent proteins and expression under the regulation of the constitutive *CaMV 35S* promoter in the thallus cells of *M. polymorpha* (Figure 16). Many of RAB GTPases whose expression was detected in the thalli exhibited similar subcellular localizations to orthologous products reported in other land plant species with a few exceptions, which suggested that this expression condition did not markedly affect the localization of the examined proteins. For example, MpRAB2a and MpRAB8 localized to the Golgi apparatus in the *M. polymorpha* thalli, whose orthologous products in Arabidopsis and tobacco were also

reported to reside on the Golgi apparatus and to function in the secretory pathway (Cheung, 2002; Speth et al., 2009; Zheng et al., 2005).

In mammalian cells, Rab1 is attached to the *cis*-Golgi membrane and endoplasmic reticulum-Golgi intermediates and functions in the early secretory pathway (Saraste et al., 1995). However, RAB1/RABD members in Arabidopsis localize at the Golgi and the TGN (Pinheiro et al., 2009). In this study, I confirmed that *M. polymorpha* RAB1 also localizes to the Golgi and the TGN. The distinct localization patterns between land plants and mammals suggest divergent functions of RAB1 homologs among eukaryotic lineages. The precise functions of RAB1/RABD members in plants at the TGN should be elucidated in future studies, and *M. polymorpha* would be a suitable material given that it harbors only two RAB1 members (Figure 3). In angiosperms, functional differentiation could have occurred in the RAB1/RABD clade: Arabidopsis RABD members are divided into two subgroups, which could function in distinct biochemical pathways in early secretory trafficking (Pinheiro et al., 2009). A comparative analysis between *M. polymorpha* and Arabidopsis would also be useful to identify the significance of the functional differentiation in this clade.

MpRAB6 was localized to the Golgi apparatus and the TGN in thallus cells. In Arabidopsis, a member of the RAB6/RABH group, RABH1b, is localized to the Golgi apparatus and unknown compartments, possibly endosomal compartments, whereas another member RABH1c is exclusively localized to the Golgi apparatus (Johansen et al., 2009). The distinct localizations of these RABH members might reflect differentiated functions of these proteins in Arabidopsis. *M. polymorpha* harbors only one member in the RAB6/RABH group, which, therefore, would be a good reference in analyses of the plant RAB6/RABH group.

The existence of two types of RAB5, the canonical RAB5 and plant-specific ARA6 groups, is an outstanding characteristic in the organization of plant RAB GTPases, which also holds true in *M. polymorpha*. In this study, I confirmed that MpRAB5 and MpARA6 localize to distinct populations of endosomes with partial overlap as described previously (Era, 2012). Whereas it is similar to the subcellular localization of Arabidopsis canonical RAB5/RABF2 and ARA6/RABF1 (Ebine et al., 2011; Ueda et al., 2004), the previous study demonstrated that the function of ARA6 could have diverged between Arabidopsis and *M. polymorpha* (Era, 2012). Furthermore, it should be noted that *M. polymorpha* harbors MpRAB21, which also localizes to the endosome. The secondary loss of RAB21 might have resulted in distinctive functional differentiation of RAB5/RABF2 and ARA6/RABF1 in descendent lineages. Rab21 is also conserved in animals (Klopper et al., 2012). However, animals do not harbor the ARA6 group, which suggests distinct coordination of endosomal RAB functions between animals and plants. It would be an intriguing project to analyze the function of MpRAB21 in *M. polymorpha*, which would elucidate how these RAB GTPases coordinate endosomal transport in *M. polymorpha* and how such mechanisms developed during land plant evolution.

It is known that the RAB11/RABA group dramatically diversified during land plant evolution. Twenty-six genes of the RAB11/RABA members are encoded in the Arabidopsis genome, which are classified into 6 subgroups (RABA1-RABA6). Although distinct functions in post-Golgi trafficking have been reported among the RABA subgroups in Arabidopsis (Choi et al., 2013; Chow et al., 2008; Kirchhelle et al., 2016), the processes and mechanisms of neofunctionalization of expanded RAB11 members remain unclear. Three *M. polymorpha* RAB11 members, MpRAB11a, MpRAB11b, and MpRAB11c, were grouped into the RABA1, RABA4, and RABA5 groups, respectively

(Figure 3, 4, and Bowman et al. 2017). It was proposed that RABA2 is an ancient subgroup of RAB11/RABA (Kirchhelle et al., 2016; Rutherford and Moore, 2002); thus, the RABA2 group may have been secondarily lost in *M. polymorpha*. Although three members of MpRAB11 have the same localization on TGNs and forming cell plates, Golgi localization was observed only for MpRAB11c. The distinct subcellular localization underpins functional differentiation among MpRAB11 members, which should be verified in future studies.

Toolbox for analyses of diversification and evolution of membrane traffic

RAB and RAB-like proteins with distinctive characteristics found in *M. polymorpha* would also be suitable tools to elucidate the mechanisms of functional diversification and neofunctionalization of RAB GTPases. MpRAB2b has an amino acid sequence similar to that of IFT43 (Figure 7), and such proteins have not been found in other eukaryotic lineages thus far. IFT43 is a subunit of the IFT-A complex involved in retrograde transport along the axoneme of cilia and flagella (Taschner et al., 2012). Other proteins similar to IFT43 have not been found in *M. polymorpha*, MpRAB2b thus may play a role in intraflagellar transport. Consistent with this notion, the expression of MpRAB2b was specifically detected in the male reproductive organ, which produces sperm equipped with flagella (Figure 8). Further localization analysis of MpRAB2b in the male reproductive organ would be needed for precise localization of this protein. This type of RAB GTPase might be specific to liverworts, given the absence of such proteins in other organisms. The genome information of neighboring species such as other liverworts and hornworts would be a good clue for clarifying whether it is specific to liverworts or not. Functional analyses of MpRAB2b would lead us to an understanding of how newly

acquired machinery components of membrane trafficking have been recruited to distinctive biological functions during plant evolution.

Another remarkable feature of the composition of RAB GTPases in *M. polymorpha* is the existence of the RAB21 and RAB23 groups, which do not exist in Arabidopsis (Figure 3). These RAB GTPases are conserved in a wide range of eukaryotic lineages, including metazoa (Klopper et al., 2012), suggesting an ancient origin for these RAB groups. Because of the secondary loss in Arabidopsis, the functions of these RAB groups in plants remain totally unexplored. It has been proposed that the last eukaryotic common ancestor possessed a larger number of RAB GTPases than extant organisms, and lineage-specific secondary loss of RAB GTPases, as well as lineage-specific acquisition of novel RAB groups, could have played important roles in diversification and specialization of membrane trafficking systems during evolution (Elias et al., 2012; Klopper et al., 2012). MpRAB21 and MpRAB23 would be sound models to identify the significance of the secondary loss of RAB GTPases during land plant evolution.

| | RAB1/RABD | RAB2/RABB | RAB6/RABH | RAB8/RABE | RAB11/RABA | | | | | | RAB5/RABF | | RAB7/RABG | RAB18/RABC | RAB21 | RAB23 |
					A1	A2	A3	A4	A5	A6	F1	F2				
Arabidopsis thaliana	4	3	5	5	9	4	1	5	5	2	1	2	8	3	-	-
Oryza sativa	3	3	2	4	6	4	2	1	2	-	2	3	4	2	1	-
Amborella trichopoda	3	2	2	2	5	3	-	2	2	1	1	3	3	2	1	-
Selaginella moellendorffii	1	1	2	2	2	1	-	2	2	-	1	1	1	1	1	1
Physcomitrella patens	3	5	7	5	-	6	-	3	3	-	3	2	3	6	5	1
Marchantia polymorpha	**2**	**2**	**1**	**3**	**1**	**-**	**-**	**1**	**1**	**-**	**1**	**1**	**1**	**1**	**1**	**1**
Klebsormidium nitens	2	1	1	1	-	1	-	-	-	-	1	1	1	1	1	1
Chlamydomonas reinhardtii	1	1	1	1	-	1	-	-	-	-	-	1	1	3	-	1
Ostreococcus tauri	1	1	1	1	-	1	-	-	-	-	1	1	1	1	1	-

Secretory RABs — Endocytic RABs — Unclassified

Figure 3. Composition of RAB GTPases in *M. polymorpha*

Number of RAB GTPases in green plants. Plant RAB GTPases are classified into 10 groups: RAB1/RABD, RAB2/RABB, RAB5/RABF, RAB6/RABH, RAB7/RABG RAB8/RABE, RAB11/RABA, RAB18/RABC, RAB21, and RAB23. RAB11/RABA and RAB5/RABF are further divided into subfamilies, RABA1-RABA6 and RABF1 and RABF2, respectively.
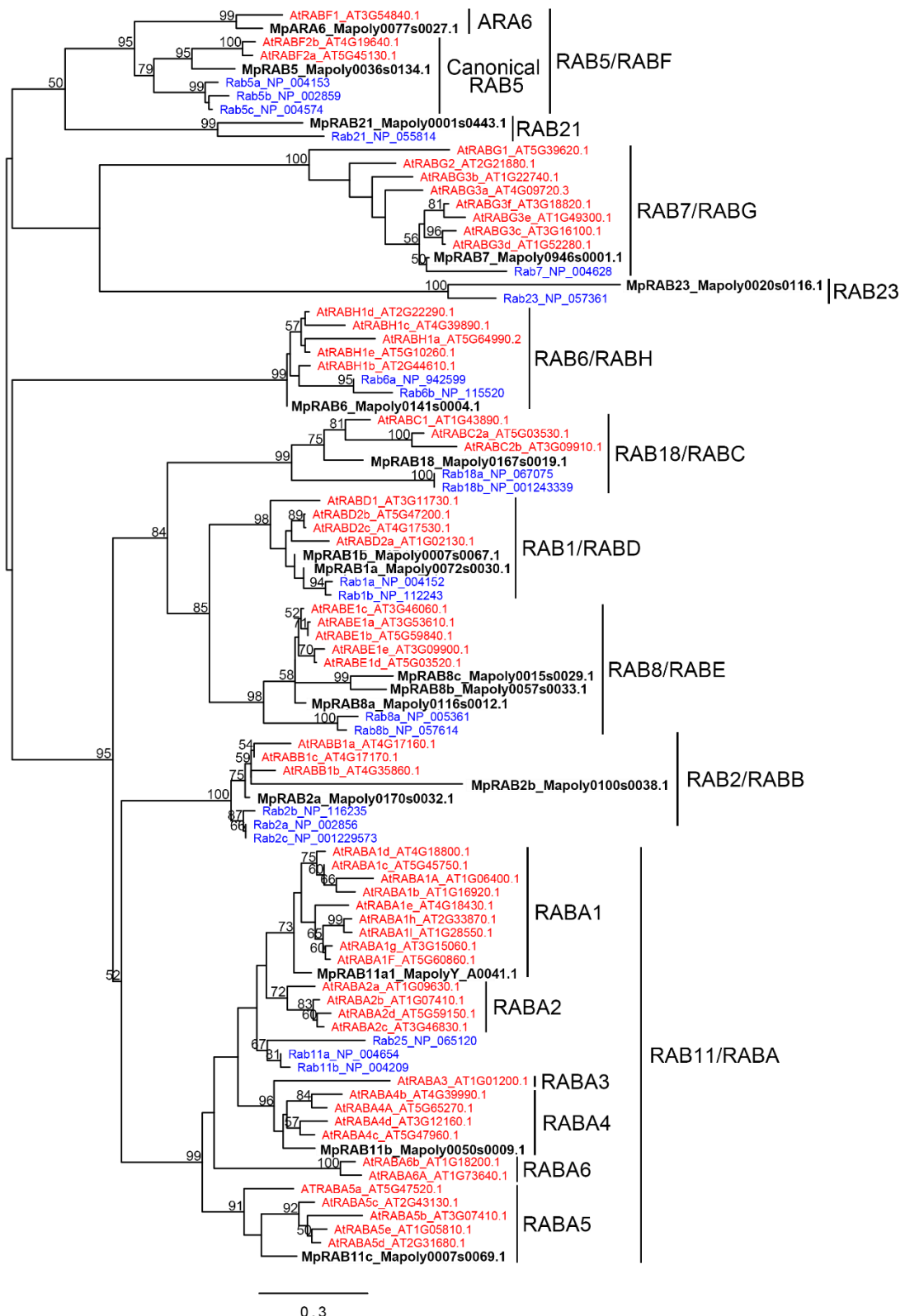
Figure 4. The maximum-likelihood phylogenetic tree of the RAB GTPases in selected

species

The maximum-likelihood phylogenetic analysis was performed using sequences of RAB GTPases from *A. thaliana*, *M. polymorpha*, and *Homo sapiens*. The bootstrap probabilities with greater than 50% support are indicated as a percentage on each branch. The color of the label is according to the species, red: *A. thaliana*, black (bold): *M. polymorpha*, blue: *H. sapiens*.

```
MpRAB11a1_MapolyY_A0041.1      MAYRSDDDYDYLFKVVLIGDSGVGKSNLLSRFTRNEFSLESKSTIGVEF
MpRAB11a2_Mapoly0018s0008.1    MAYRSDDDYDYLFKVVLIGDSGVGKSNLLSRFTRNEFSLESKSTIGVEF
                               ************************************************

MpRAB11a1_MapolyY_A0041.1      ATRSINVDSKLIKAQIWDTAGQERYRAITSAYYRGAVGALLVYDITRHV
MpRAB11a2_Mapoly0018s0008.1    ATRSINVDSKLIKAQIWDTAGQERYRAITSAYYRGAVGALLVYDITRHV
                               ************************************************

MpRAB11a1_MapolyY_A0041.1      TFENVERWLKELKDHTDSNIVVMLVGNKSDLRHLRAVSTDDGQSFSEKE
MpRAB11a2_Mapoly0018s0008.1    TFENVERWLKELKDHTDSNIVVMLVGNKSDLRHLRAVSTDDGQNFSEKE
                               *******************************************  *****

MpRAB11a1_MapolyY_A0041.1      SLFFMETSALESTNVENAFKQILTQIYRVVSKKALDVGEDPSAGPGKGQ
MpRAB11a2_Mapoly0018s0008.1    SLFFMETSALESTNVENAFKQILTQIYRVVSKKALDVGEDPSAGPGKGQ
                               ************************************************

MpRAB11a1_MapolyY_A0041.1      TIQVGNKDEVTATKKVGCCSA
MpRAB11a2_Mapoly0018s0008.1    TITVGNKDEVTATKKVGCCSA
                               ** *****************
```

Figure 5. Alignment of sequences of MpRAB11a1 and MpRAB11a2

Amino acid sequences of MpRAB11a1 (MapolyY_A0041.1) and MpRAB11a2 (Mapoly0018s.0008.1) are aligned. Asterisks indicate identical amino acid residues.
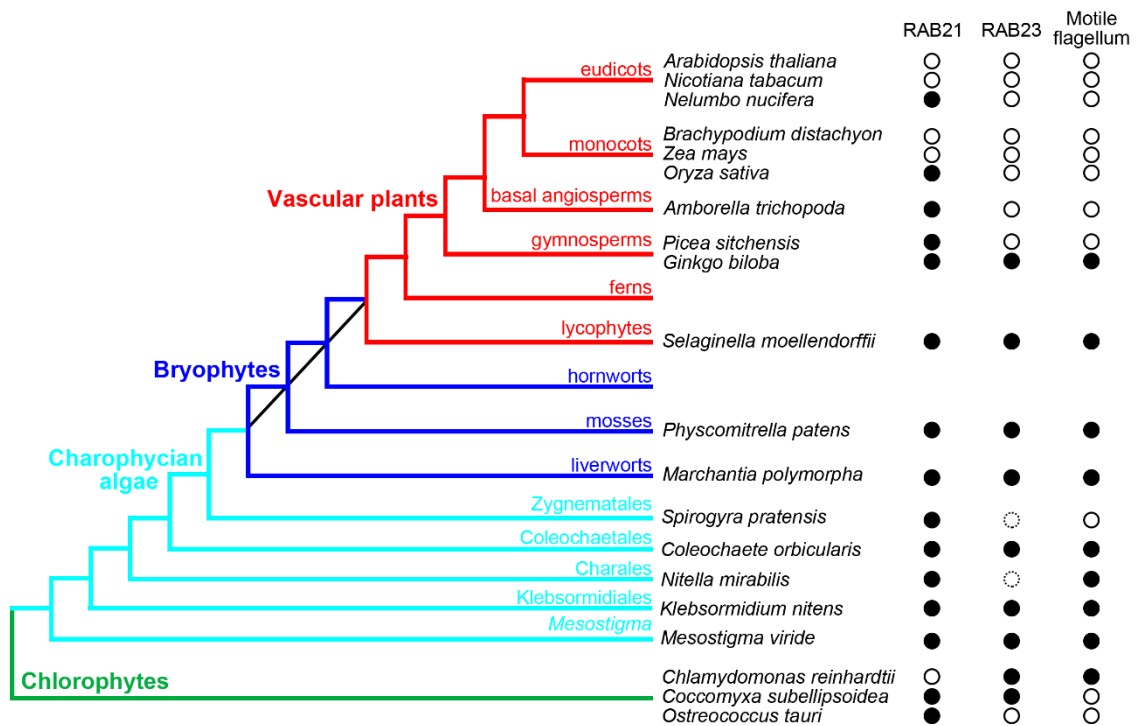
47

Figure 6. Distribution of *RAB21* and *RAB23* genes in green plants

Distribution of *RAB21* and *RAB23* genes in representative species of green plants is shown. Red, blue, cyan, and green colors in the phylogenic tree indicate vascular plants, bryophytes, charophytes, and chlorophytes, respectively. A black line indicates that phylogenetic relationship of bryophytes has been unresolved. Black circles and white circles indicate the presence and absence of genes, respectively. Dotted-line circles indicate that genes are not found in transcriptomes publicly available.
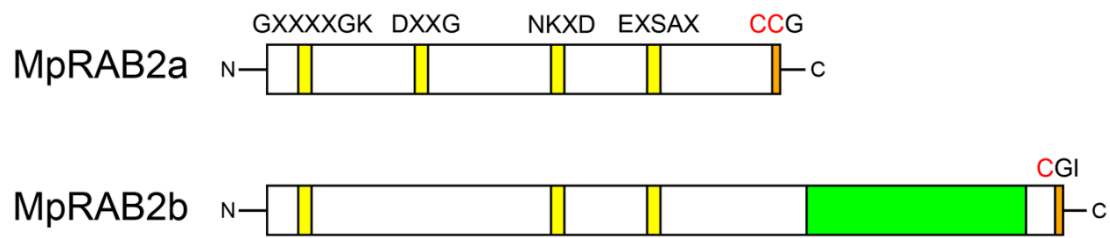
Figure 7. The schematic diagram of primary sequences of MpRAB2a and MpRAB2b

Yellow boxes indicate amino acid sequences conserved in the Ras superfamily (GXXXXGK, DXXG, NKXD, and EXSAX). A green box indicates the region similar to IFT43, and the orange boxes indicate predicted lipid modification sites.
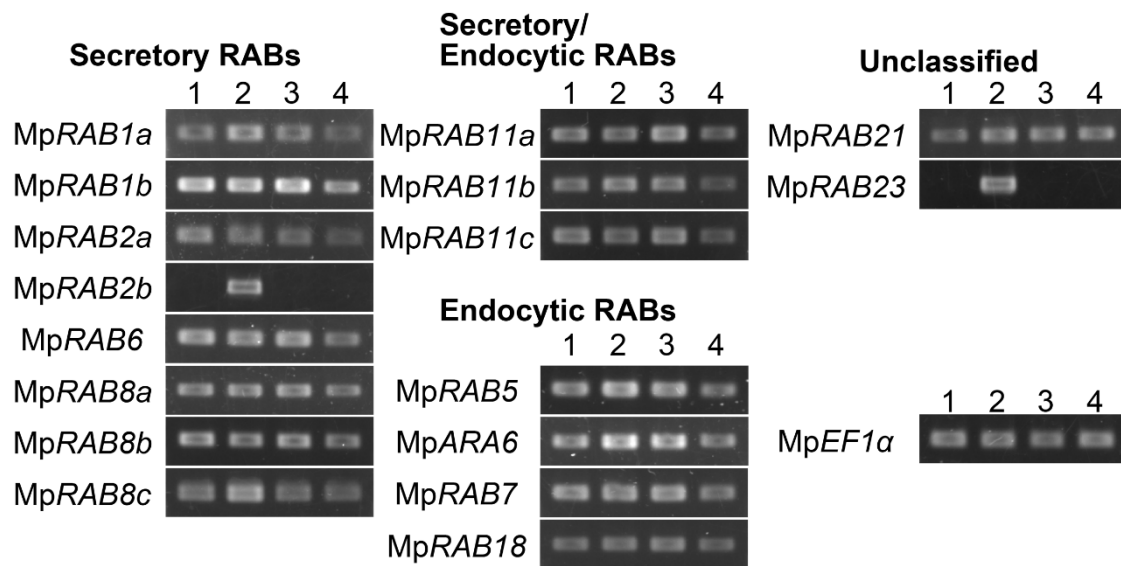
Figure 8. Transcription patterns of *M. polymorpha* RAB GTPase genes

Total RNA products were prepared from 5-day-old thalli (lane 1), antheridiophores (lane 2), archegoniophores (lane 3), and 7-day-old sporelings (lane 4). The amount of template cDNA was adjusted with the Mp*EF1α* expression. Primer sets and cycles for PCR are listed in Materials and Methods.
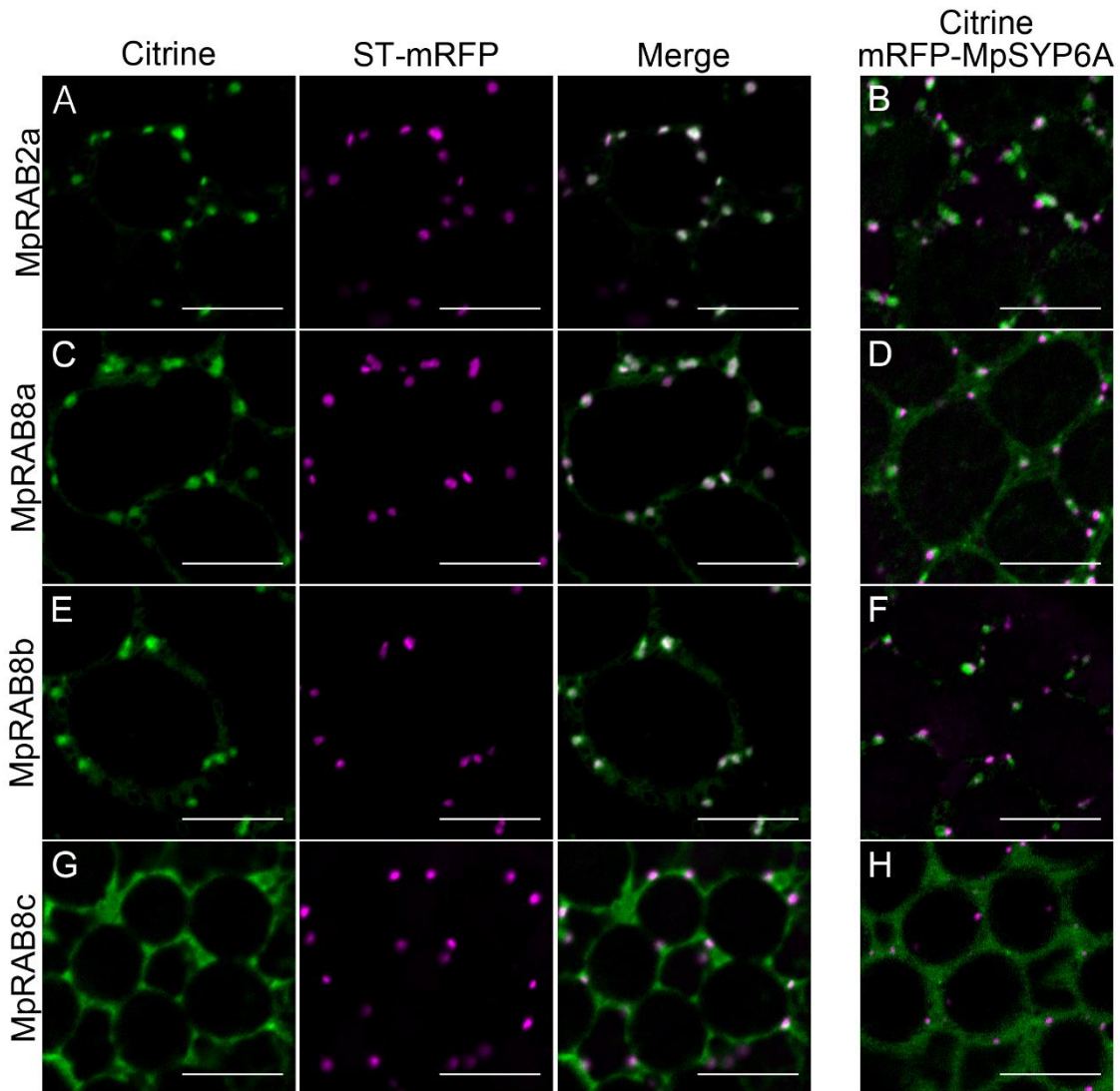
Figure 9. Golgi apparatus-localized RAB GTPases in *M. polymorpha*

Colocalization of Golgi-localized RAB GTPases with the marker for the Golgi apparatus (ST-mRFP) or the TGN (mRFP-MpSYP6A). (A, C, E, and G) Single confocal images of thallus cells expressing ST-mRFP (magenta) and Citrine-MpRAB2a (A), Citrine-MpRAB8a (C), Citrine-MpRAB8b (E), or Citrine-MpRAB8c (G) (green). (B, D, F, and H) Single confocal images of thallus cells expressing mRFP-MpSYP6A (magenta) and Citrine-MpRAB2a (B), Citrine-MpRAB8a (D), Citrine-MpRAB8b (F), or Citrine-MpRAB8c (H).   Scale bars = 10 μm.
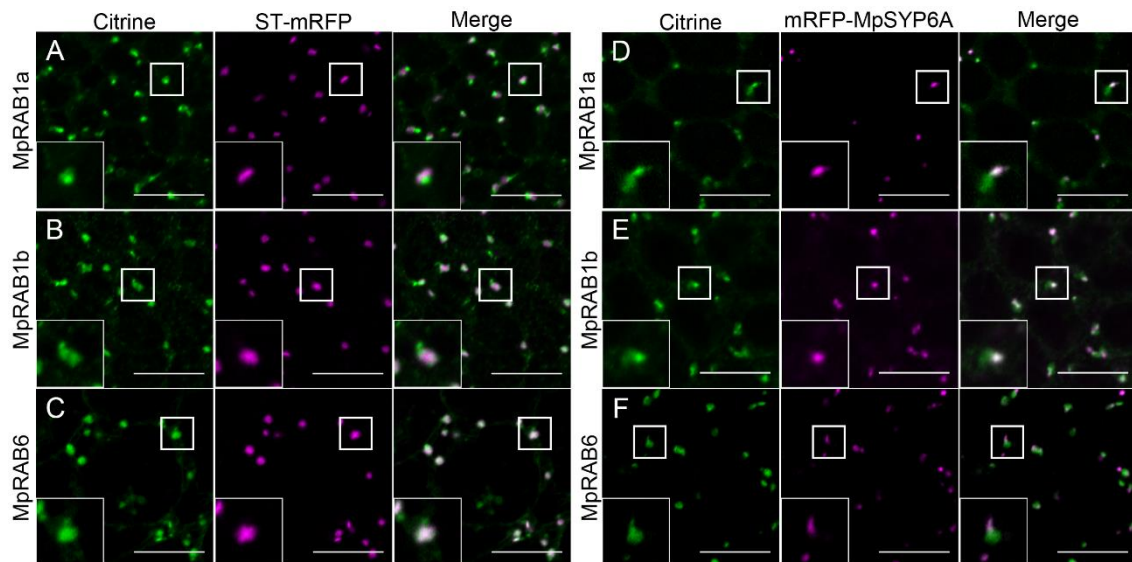
Figure 10. Subcellular localization of MpRAB1 and MpRAB6 members

(A, B, and C) Single confocal images of thallus cells expressing ST-mRFP (magenta) and Citrine-MpRAB1a (A), Citrine-MpRAB1b (B), or Citrine-MpRAB6 (C) (green). (D, E, and F) Single confocal images of thallus cells expressing mRFP-MpSYP6A (magenta) and Citrine-MpRAB1a (D), Citrine-MpRAB1b (E), or Citrine-MpRAB6 (F) (green). Insets are higher magnification images of squared areas. Scale bars = 10 μm.
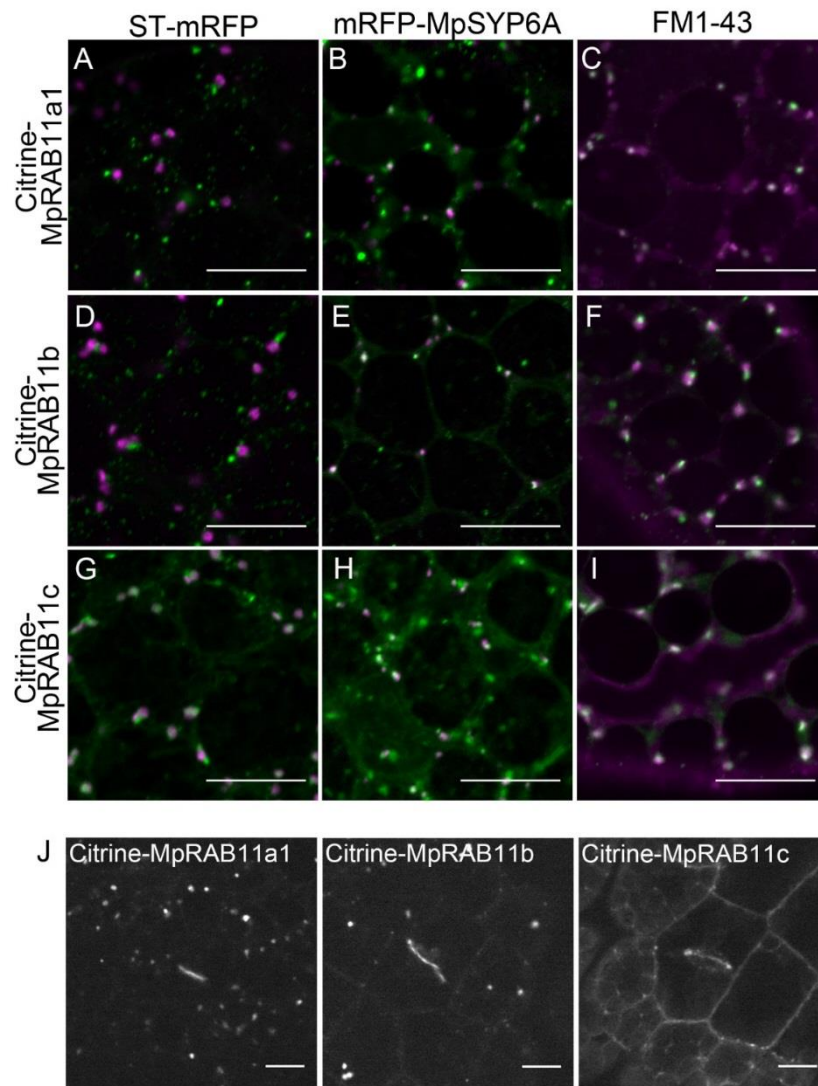
Figure 11. Subcellular localization of MpRAB11 members

(A, D, and G) Single confocal images of thallus cells expressing ST-mRFP (magenta) and Citrine-MpRAB11a1 (A), Citrine-MpRAB11b (D), or Citrine-MpRAB11c (G) (green). (B, E, and H) Single confocal images of thallus cells expressing mRFP-MpSYP6A (magenta) and Citrine-MpRAB11a1 (B), Citrine-MpRAB11b (E), or Citrine-MpRAB11c (H) (green). (C, F, and I) Single confocal images of thallus cells expressing Citrine-MpRAB11a (C), Citrine-MpRAB11b (F), or Citrine-MpRAB11c (I) (green) stained with FM1-43 (magenta). (J) Single confocal images of forming cell plates with Citrine-MpRAB11 members. Scale bars = 10 μm.
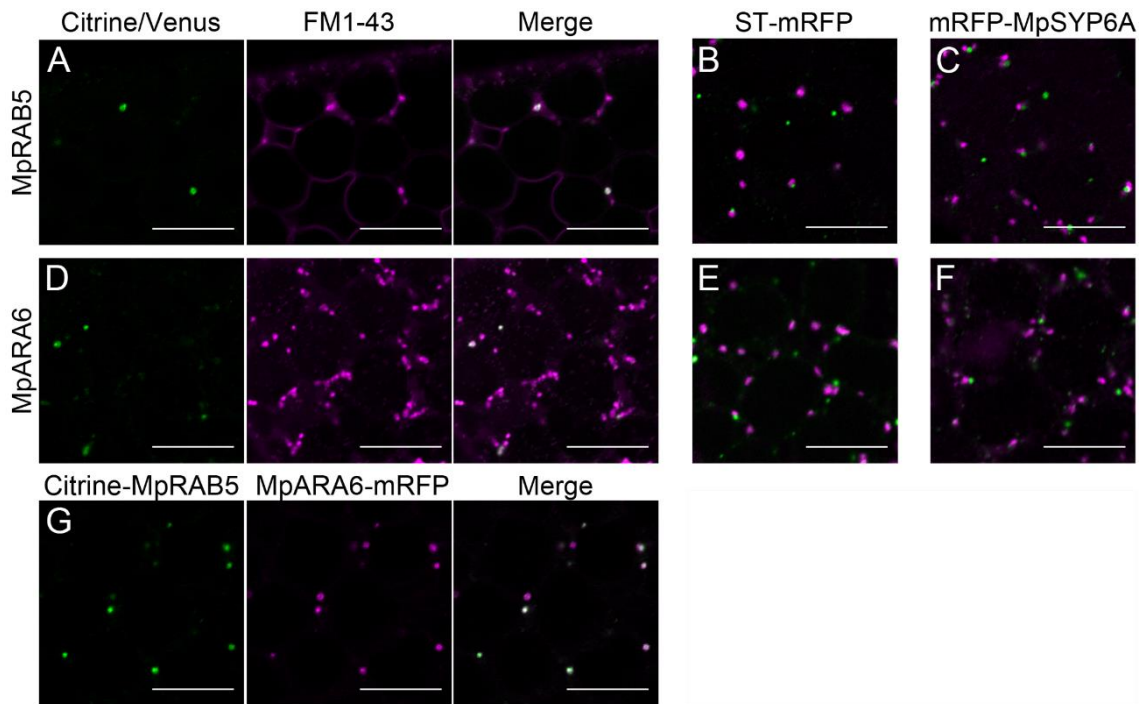
Figure 12. Subcellular localization of MpRAB5 and MpARA6

(A and D) Single confocal images of thallus cells expressing Citrine-MpRAB5 or MpARA6-Venus (green) stained with FM1-43 (magenta). (B and E) Single confocal images of thallus cells expressing ST-mRFP (magenta) and Citrine-MpRAB5 or MpARA6-Citrine (green). (C and F) Single confocal images of thallus cells expressing mRFP-MpSYP6A (magenta) and Citrine-MpRAB5 or MpARA6-Citrine (green). (G) Single confocal images of a thallus cell expressing Citrine-MpRAB5 (green) and MpARA6-mRFP (magenta). Scale bars = 10 μm.
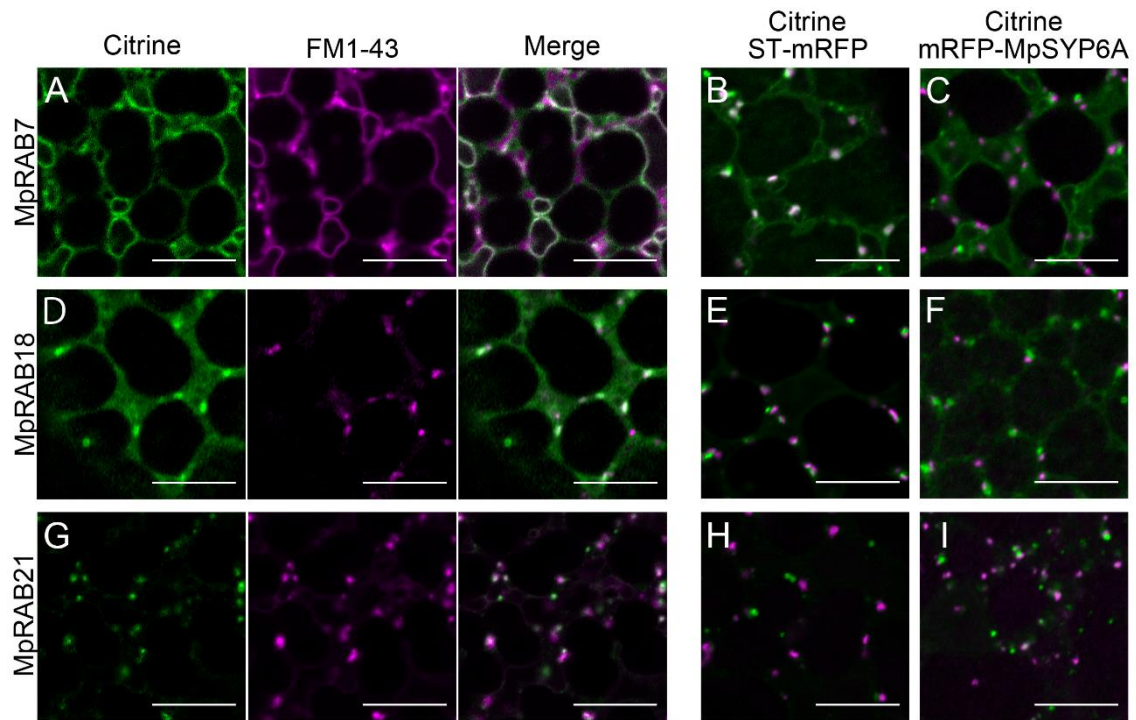
.

Figure 13. RAB GTPases localized to endocytic compartments

(A, D, and G) Single confocal images of thallus cells expressing Citrine-MpRAB7 (A), Citrine-MpRAB18 (D), or Citrine-MpRAB21 (G) (green) stained with FM1-43 (magenta). (B, E, and H) Single confocal images of thallus cells expressing ST-mRFP (magenta) and Citrine-MpRAB7 (B), Citrine-MpRAB18 (E), or Citrine-MpRAB21 (H) (green). (C, F, and I) Single confocal images of thallus cells expressing mRFP-MpSYP6A (magenta) and Citrine-MpRAB7 (C), Citrine-MpRAB18 (F), or Citrine-MpRAB21 (I) (green). Scale bars = 10 μm.
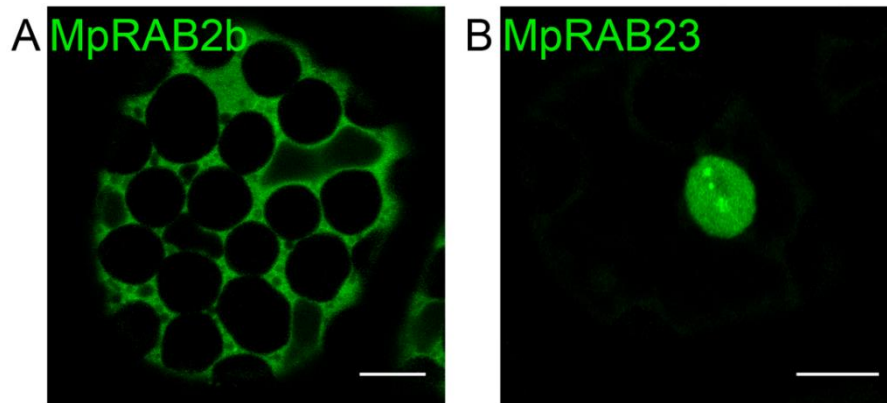
Figure 14. Subcellular localization of MpRAB2b and MpRAB23 ectopically expressed in thallus cells

(A) A single confocal image of thallus cells expressing Citrine-MpRAB2b. (B) A single confocal image of thallus cells expressing Citrine-MpRAB23. Scale bars = 10 μm.

```
MpRAB23

MLSMQEEDFEREVKVVVVGNGCVGKTSMIRQFCKGVYANEY

KKTIGVDFLEKLQFVRGLDEEVKMMLWDTAGQEQFHALTRA

YYRGARAAALCFSTIDRDSFEAIRTWKEKVEEECGQIPMVL

VQNKVDLLENAVVSRQEAEDLATELGLRFYRICVKENLYVA

DVFEYLAEMYLQKDMRIYHCQPRPNITKAVASRIATSAPPQ

VDMKVDTVCKRSKVINIRKRRRRRLQSECSIL
```

Figure 15. The amino acid sequence of MpRAB23

The region indicated in red is the NLS-like domain predicted by cNLS Mapper.
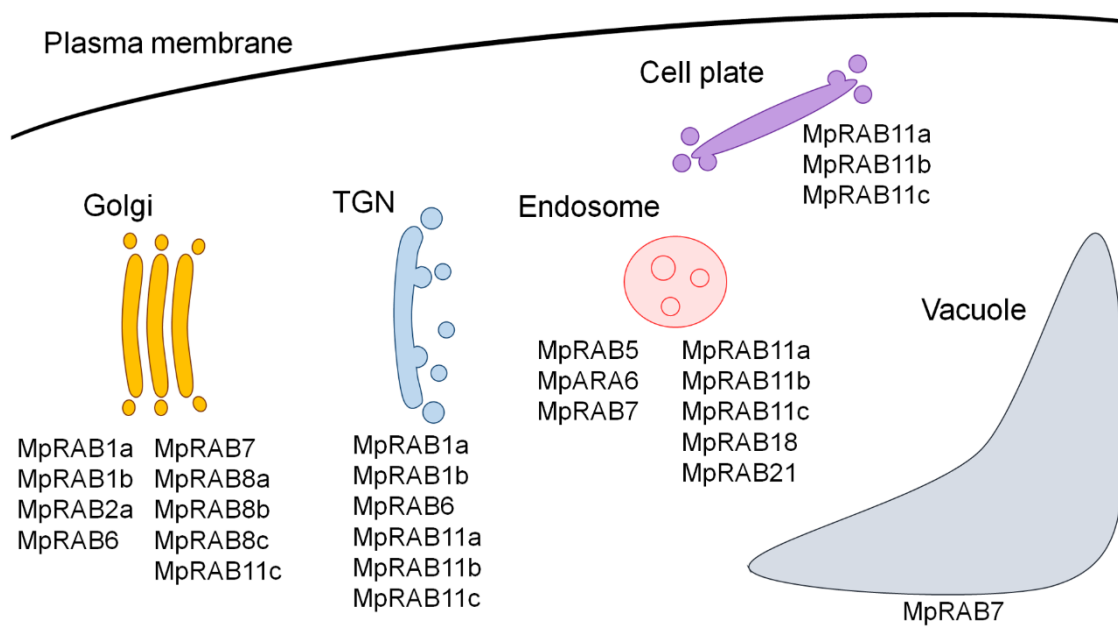
Figure 16. Subcellular distribution of RAB GTPases expressed in thallus tissues of *M. polymorpha*

Chapter 2

Functional analyses of RAB21 in *M. polymorpha*

本章については，5 年以内に雑誌等で刊行予定のため，非公開.

Chapter 3

Organelle dynamics during spermatozoid formation and RAB23 functions in *M. polymorpha*

Introduction

The RAB23 group is secondarily lost during land plant evolution. Animal RAB23 is essential for viability and plays critical roles in Sonic hedgehog (Shh) signaling (Eggenschwiler et al., 2001). It has been also shown that RAB23 is involved in cilia formation, and ciliary transport of Smoothened (Boehlke et al., 2010; Yoshimura et al., 2007). In *Trypanosoma brucei*, RAB23 is localized to the flagellum (Lumb and Field, 2011). These facts strongly suggest that RAB23 is required for normal ciliary and flagellar functions. Consistently, RAB23 is highly conserved in organisms possessing motile cilia and/or flagella (Lumb and Field, 2011), which also holds true in plant lineages: RAB23 is conserved in plants that use flagella-equipped gametes for sexual reproduction (Chapter 1, and Bowman et al., 2017). However, the precise molecular function of RAB23 still remains ambiguous.

Some plant lineages including liverworts generate motile sperms called spermatozoids as male gametes, each of which harbors a helical cell body and two or more motile flagella (Figure 31A). A common feature of the plant spermatozoids is a helically shaped cell body, which confers the name "Streptophyta" to the taxon consisting of charophytes and land plants (Embryophyta). The architecture of plant spermatozoids has been investigated by many electron microscopic studies (Carothers and Kreitner, 1968; Graham and McBride, 1979; Li et al., 1989; Renzaglia and Duckett, 1987; Renzaglia and Garbary, 2001; Ueda, 1979; Vaughn and Renzaglia, 2006), which revealed that the spiral morphology is rendered by the spline, which is a band of microtubules extending from the multilayered structure (MLS) located at the apical region of the spermatozoid. The MLS is characteristic to spermatozoids formed in Streptophyta, above which basal bodies associated with flagella are located (Carothers and Kreitner, 1968;

Graham and McBride, 1979; Li et al., 1989; Renzaglia and Duckett, 1987). The number of flagella is divergent among land plants: bryophytes and some pteridophytes generate biflagellate spermatozoids, while spermatozoids of other pteridophytes and some gymnosperms harbor larger numbers of flagella (Renzaglia and Garbary, 2001).

The liverwort, *M. polymorpha* is a suitable model organism representing basal land plants to analyze plant spermatozoids. The processes of spermatozoid formation (spermatogenesis) have been described through histological observations. Antheridia, which are composed of outer jacket cells and inner reproductive cells, are buried in antheridial receptacles (Figure 31B). Within an antheridium, spermatogenous cells divide transversely and vertically to increase the number of cells that form spermatid mother cells. A spermatid mother cell then divides diagonally to generate two spermatids, which then undergo transformation into the individual spermatozoid (Figure 31C and (Shimamura, 2016). The transformation sequence is accompanied by complete morphological alteration in a process called spermiogenesis. Spermiogenesis in liverworts comprises various dynamic cellular events including reduction of the cytoplasm, condensation of the nucleus, replacement of organelles, and formation of the locomotory apparatus (Renzaglia and Duckett, 1987; Renzaglia and Garbary, 2001; Ueda, 1979). The completion of spermiogenesis culminates in the formation of mature spermatozoids, which are released into the water and move towards the female gametes produced in the female reproductive organ, the archegoniophore. The process of sperm development in liverworts has been of great interest to cell and developmental biologists (Higo et al. 2016; Renzaglia and Garbary 2001). However, details of cell and organelle dynamics during plant spermatogenesis remain largely unknown. This is in part because

of a lack of appropriate tools with which to visualize cellular dynamics and structures in cells undergoing spermatogenesis.

In this study, I firstly investigated organelle dynamics during spermatogenesis in *M. polymorpha* using fluorescently tagged SNARE proteins, RAB GTPases, and flagellar components as organelle markers. I then attempted to uncover the function of MpRAB23 in *M. polymorpha* through genetic and cell biological studies, which demonstrated that MpRAB23 is essential for formation and function of the spermatozoid in *M. polymorpha*.

Results

Dynamic relocalization of MpSYP1 members during spermiogenesis

Given a conserved function of RAB GTPases in membrane trafficking and the specific expression in the male reproductive organ, RAB23 could be involved in membrane trafficking and/or organelle dynamics during spermatogenesis in *M. polymorpha*. Therefore, I observed behaviors of organelle markers during spermatogenesis. To analyze morphological changes in cells undergoing spermatogenesis, I firstly visualized cell shapes using a fluorescent marker targeted to the plasma membrane. To achieve this, I employed mCitrine-MpSYP12A, which is a member of the SYP1 group mediating membrane fusion at the plasma membrane (Kanazawa et al., 2016; Sanderfoot, 2007). In thallus cells, mCitrine-MpSYP12A driven by its own promoter was localized on the plasma membrane (Figure 32A). However, I did not detect any fluorescence from mCitrine-MpSYP12A on the plasma membrane of the spermatozoid (Figure 32B). I then examined if I could detect mCitrine-MpSYP12A in actively dividing spermatogenous cells and found that mCitrine-MpSYP12A was expressed at this stage and was localized to the plasma membrane (Figure 32C). These results suggested that mCitrine-MpSYP12A

is degraded during spermatozoid formation in *M. polymorpha*. To determine the stage at which mCitrine-MpSYP12A disappears from the plasma membrane, I observed spermatogenous tissues at different stages of spermatogenesis. Since antheridia are aligned from young to mature starting from the edge of the antheridiophore (Shimamura, 2016), I could observe antheridia at different developmental stages in a single antheridiophore. Plasma membrane localization of mCitrine-MpSYP12A was also observed in spermatids just after the last cell division occurred in a diagonal direction. The localization on punctate structures in the cytoplasm was also detected (Figure 32D). When the cytoplasm of spermatids began to shrink, the plasma membrane localization of MpSYP12A was gradually decreased. Instead, large spherical structures containing mCitrine fluorescence became evident in the cytoplasm (Figure 32E). In the later stage, MpSYP12A completely disappeared from the plasma membrane and instead accumulated in the spherical structures (Figure 32F).

To examine whether this relocalization from the plasma membrane to the spherical structures was an event specific to MpSYP12A, I examined the subcellular localization of another SYP1 member, MpSYP13A. While mCitrine-MpSYP13A was localized almost exclusively in the plasma membrane during the proliferative phase (Figure 32G), it accumulated only in the spherical structures at the later stages (Figure 32H). These results indicated that the protein content of the plasma membrane was completely reorganized during spermiogenesis in *M. polymorpha*.

Other organelle proteins also accumulate in the spherical structures

To observe the behavior of other organelles during spermatogenesis, I observed transgenic lines of *M. polymorpha* expressing a fluorescently tagged Golgi-resident

SNARE protein, MpGOS11, under the regulation of the Mp*SYP2* promoter (mCitrine-MpGOS11) (Kanazawa et al., 2016), or mCitrine-MpRAB5, driven by its own promoter. mCitrine-MpGOS11 was localized to the disc- or ring-shaped structures during the early stages of antheridia development (Figure 33A). At the later stages of antheridia development, during spermiogenesis, mCitrine-MpGOS11 accumulated in the larger spherical structures similar to the observations with MpSYP12A and MpSYP13A (Figure 33B). Similar translocation from punctate structures in the cytoplasm to larger spherical structures during spermiogenesis was also observed for mCitrine-MpRAB5 (Figure 33C and 33D). These data suggested that the organelles and cytoplasmic components including the Golgi apparatuses and endosomes were transported to the spherical structures during spermatogenesis. I considered that these spherical structures represent vacuoles because of their sizes and spherical shapes. Therefore, I next observed the transgenic plants expressing mCtirine-MpVAMP71 or mCitrine-MpSYP2, which were vacuolar SNARE proteins, under the regulation of their own promoters. Both of these SNARE proteins were localized at the vacuolar membrane during the early stages of antheridia development (Figure 33E and 2H) and were localized to the membrane on the larger spherical structures in later stages (Figure 33F and 33I). These results showed the vacuolar nature of the spherical structures. Intriguingly, the localization of mCitrine-MpSYP2 fluorescence changed from being limited to the membrane of the spherical structures to including the luminal spaces as spermiogenesis progressed (Figure 33J), whereas mCitrine-MpVAMP71 remained on the membrane of the spherical structures (Figure 33G). The distinct dynamics of the two vacuolar SNARE proteins may indicate that these two SNAREs play different roles during spermiogenesis.

Degradative organelles observed in spermatids undergoing spermiogenesis

To obtain more information on the spherical structures, I performed electron microscopic observations of the developing antheridia. Antheridia from antheridiophores were divided into two groups according to their developmental stages, those at the young stage and those at the maturing stage. The samples at the young stage contained antheridia that had dividing spermatogenous cells, spermatid mother cells, and spermatids before shrinkage of the cytoplasm but contained no spermatids undergoing spermiogenesis (Figure 34A). Antheridia at the maturing stage contained spermatids undergoing spermiogenesis and were associated with shrinking cytoplasm (Figure 34B). Spermatids at the maturing stage contained large vacuole-like compartments with sizes comparable to those of the spherical structures observed in fluorescence microscopy (Figure 34B). The MVEs were also observed in the spermatids (Figure 34C), suggesting that the endocytic degradation pathway was active during spermiogenesis. Notably, autophagy-related structures such as autophagosomes (Figure 34D) and autophagic bodies (Figure 34E) were observed frequently in antheridia cells at the maturing stage. I also observed vacuoles containing the Golgi apparatus in the luminal space (Figure 34F and 33G), suggesting that active degradation of cytoplasmic components including whole organelles occurred during spermiogenesis. The enhanced autophagic degradation during spermiogenesis was also supported by the result of quantification. A significantly larger number of autophagosomes was observed in cells in the maturing stage than in the young stage (Figure 34H). These results indicate that autophagy became highly active and degraded cytoplasmic components during spermiogenesis in *M. polymorpha*. I also noted that autophagic bodies and residuals of the cytosol were present between the plasma membrane of shrinking cell bodies and the cell wall (arrowheads in Figure 34D). These

might represent remnants of cytoplasm that are internalized into the spherical structures by the autophagic processes and released during fusion between the membrane of spherical structures and the plasma membrane of spermatids.
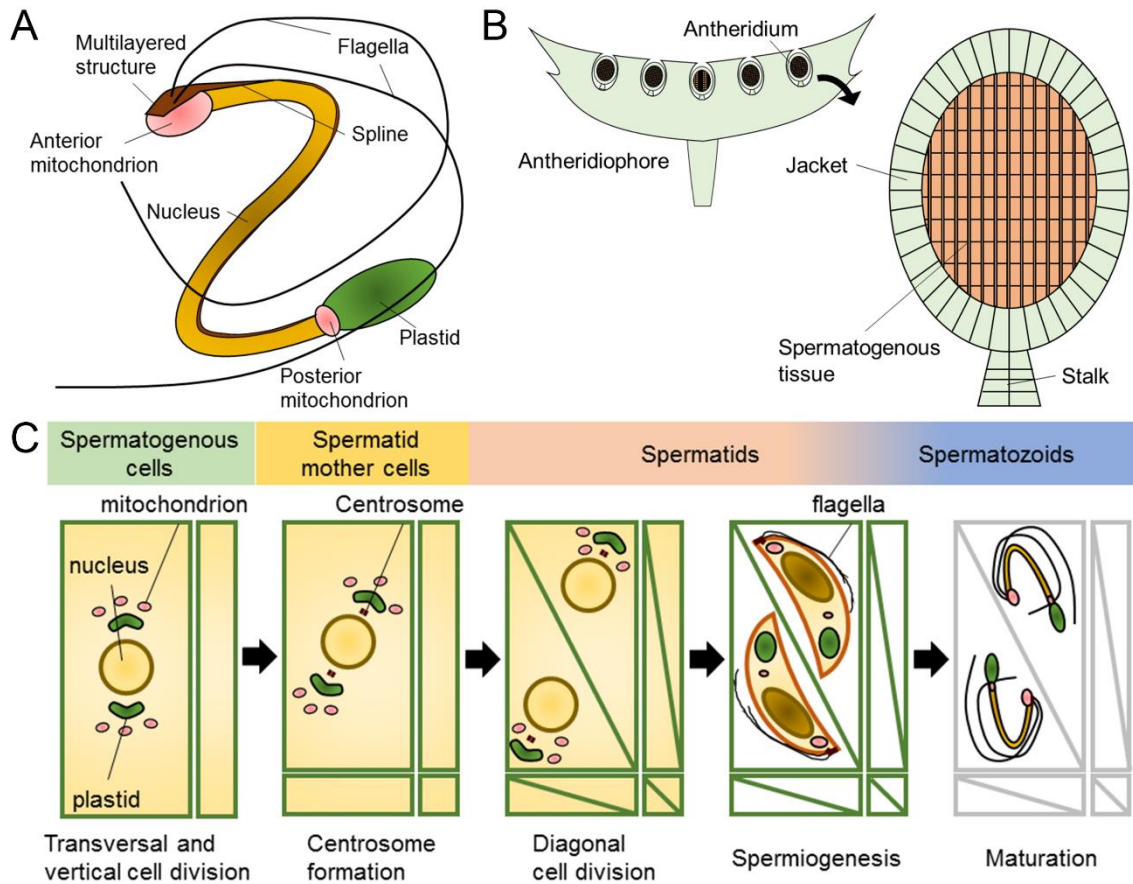
本章の以降の部分については，5 年以内に雑誌等で刊行予定のため，非公開．

Figure 31. Spermatozoid architecture and development of _M. polymorpha_

(A) A diagram of the spermatozoid of _M. polymorpha._ The cell body of a spermatozoid possesses a helical shape and contains an elongated nucleus and some organelles and subcellular structures. At the anterior region, there are a large mitochondrion, a multilayered structure (MLS), and two basal bodies from which motile flagella elongate. An upper layer of the MLS is a spline, which is a band of microtubules and elongates along the nucleus to act as a framework of the helical shape of the spermatozoid. The posterior region contains a posterior mitochondrion and a large plastid. (B) Drawing of an antheridium of _M. polymorpha_. In an antheridium, the spermatogenous tissue is surrounded by outer jacket cells (jackets). Each antheridium is connected with the antheridiophore by a stalk. (C) Scheme of spermatozoid formation of _M. polymorpha_. In

111

the spermatogenous tissue, spermatogenous cells divide transversely and vertically to increase the number of cells to form spermatid mother cells. Centrosomes are newly synthesized in spermatid mother cells. Spermatid mother cells divide diagonally to generate spermatids, and spermatids then undergo dynamic morphological changes called spermiogenesis, and transform into spermatozoids.
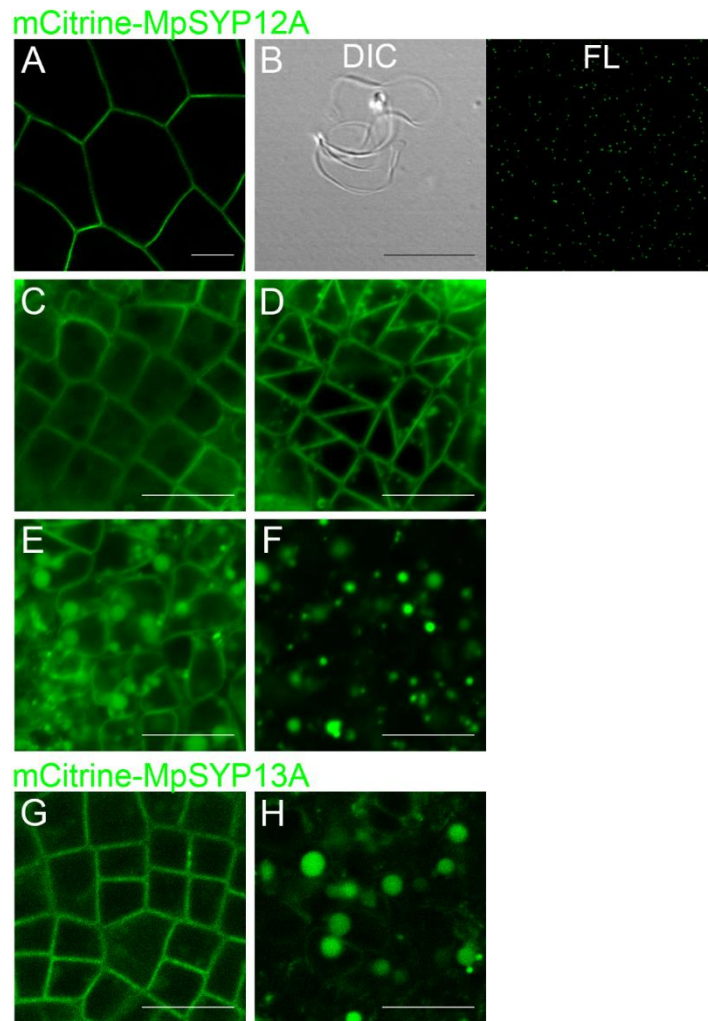
Figure 32. Relocalization of PM-proteins during spermatogenesis

(A) mCitrine-MpSYP12A localized on the plasma membrane (PM) in thallus cells. (B) Differential interference contrast (DIC) and fluorescent (FL) images of a spermatozoid collected from the transgenic line expressing mCitrine-MpSYP12A. Green dots in the FL image are image noise. (C, D, E, and F) Relocalization of mCitrine-MpSYP12A during spermatogenesis. Single confocal images were aligned in a young-to-mature order. (G and H) Subcellular localization of mCitrine-MpSYP13A at the young (G) and mature (H) stages during spermatogenesis. Scale bars = 10 μm.
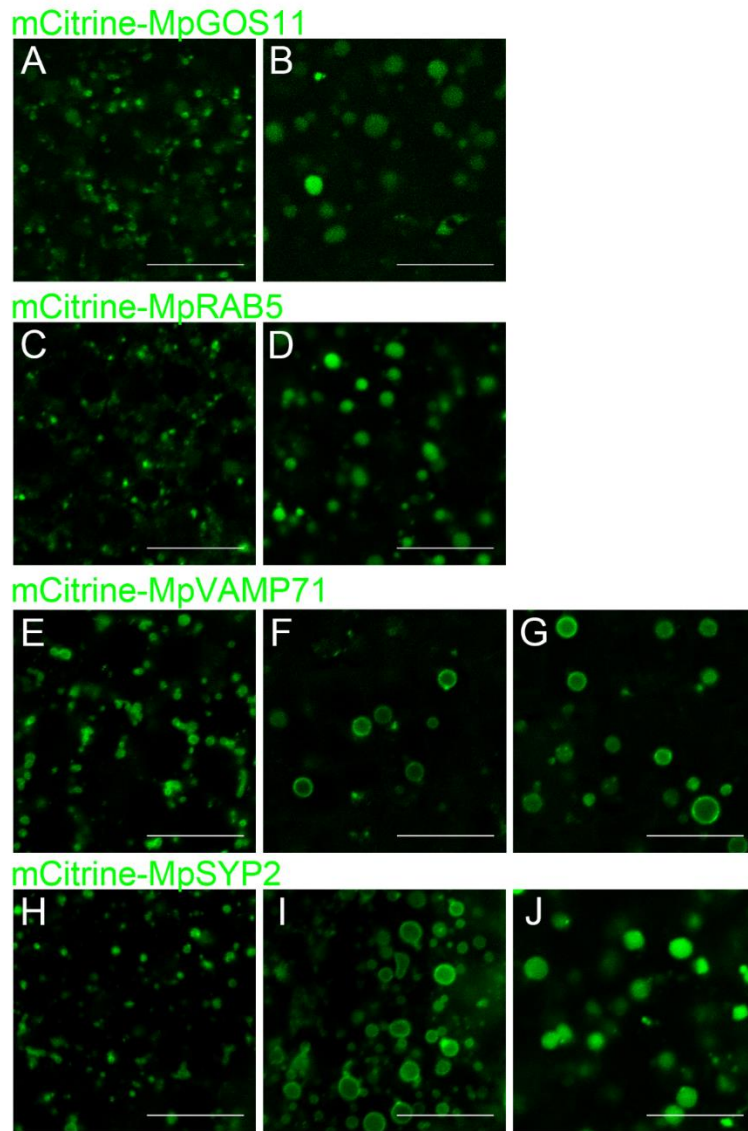
Figure 33. Dynamic relocalization of organelle markers during spermatogenesis

(A and B) Subcellular localization of mCitrine-MpGOS11 in the early (A) and late (B) stages of spermatogenesis. (C and D) Subcellular localization of mCitrine-MpRAB5 in the early (C) and late (D) stages of spermatogenesis. (E, F, and G) Subcellular localization of mCitrine-MpVAMP71 in the early (E) and late (F and G) stages of spermatogenesis. (H, I, and J) Subcellular localization of mCitrine-MpSYP2 in the early (H) and late (I and J) stages of spermatogenesis. Scale bars = 10 μm.
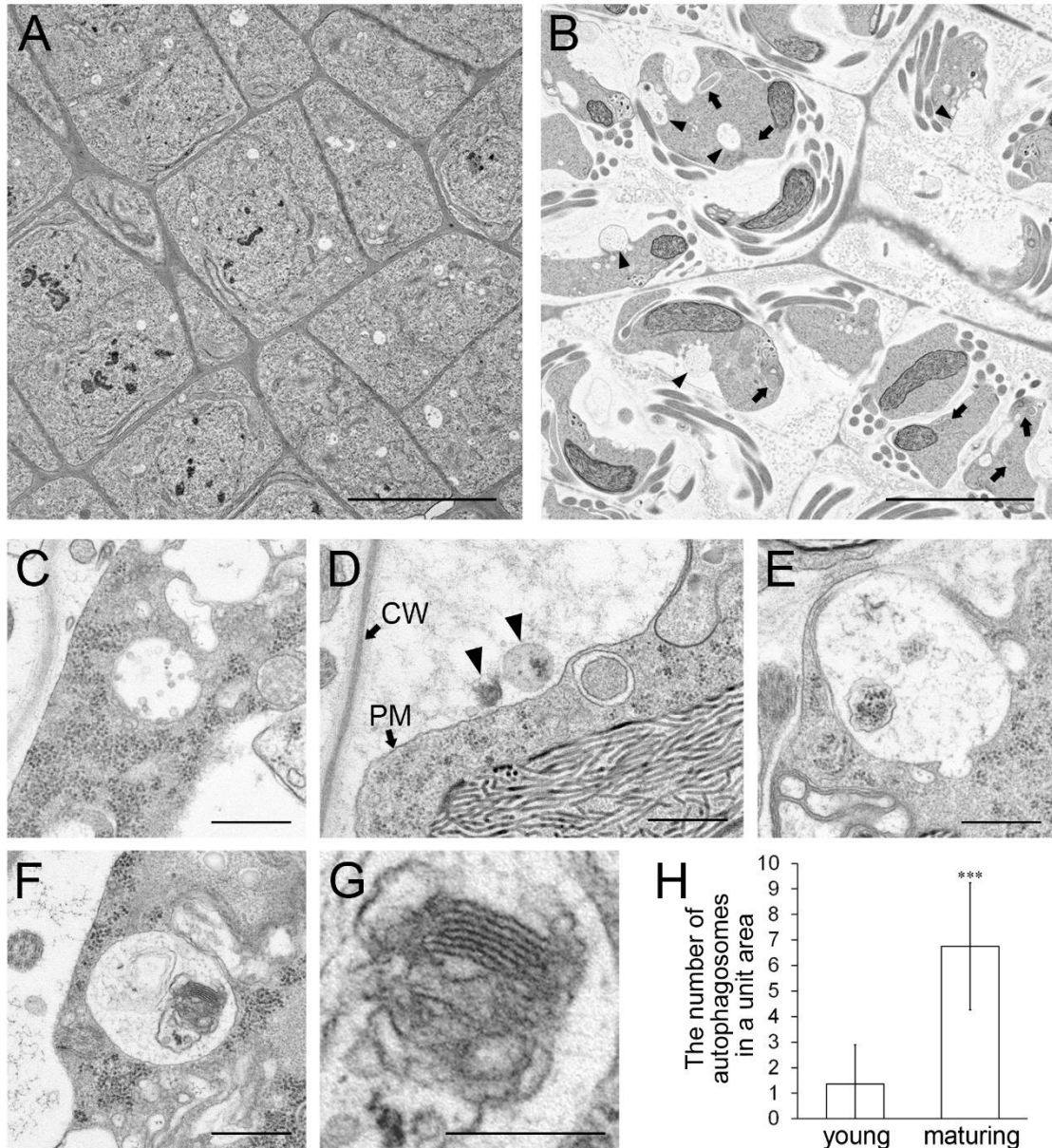
Figure 34. Electron microscopic observation of antheridial cells in *M. polymorpha*

(A) An image of spermatogenous cells of *M. polymorpha*. (B) An image of spermatid cells of *M. polymorpha*. Arrowheads and arrows indicate spherical structures and autophagosomes, respectively. (C) Multivesicular endosomes in the spermatid undergoing spermiogenesis. (D) Autophagosomes were frequently observed in spermatids undergoing spermiogenesis. Arrowheads indicate an autophagic body-like structure (right) and remnants of the cytoplasm (left) in the paramural space. Arrows

indicate the cell wall (CW) and plasma membrane (PM). (E) An autophagic body in the luminal space of a spherical structure. (F) The Golgi apparatus in the luminal space of a spherical structure. (G) A high magnification image of the Golgi apparatus shown in (F). Scale bars = 5 μm (A, B), 500 nm (C-F), and 250 nm (G). (H) The average number of autophagic structures in a unit area (24.9 μm × 24.9 μm). Cells were classified into two groups; young cells (young) in which the cytoplasm was not shrunk (n = 11 images), and maturing cells (maturing) in which the cytoplasm was shrinking (n = 8 images). ***P <0.001, Student's t test.

本章の以降の部分については，5 年以内に雑誌等で刊行予定のため，非公開.

General Discussion

Recent genomic analyses proposed that diversification and specialization of membrane trafficking components including RAB GTPases are closely associated with diversification of the membrane trafficking system during evolution, which could be also associated with diversification of physiology and/or development of eukaryotes (Dacks and Field, 2007). Also for land plant evolution, it is speculated that the expansion of membrane trafficking components is tightly related to terrestrialization and/or multicellularization (Rutherford and Moore, 2002; Sanderfoot, 2007), which, however, was not properly supported because of limited information from basal land plant species. In this study, I made use of the emerging model liverwort, *M. polymorpha*, to address this subject through studies of RAB GTPases, which is a key machinery component of membrane trafficking. I identified all genes for RAB GTPases in the *M. polymorpha* genome, which revealed that *M. polymorpha* possesses a fundamental set of RAB GTPases conserved in green plants with low redundancy. I also found that the repertoire of RAB GTPases in *M. polymorpha* is clearly distinct from those in other land plants. A sound example is the number of RAB11/RABA members. *M. polymorpha* harbors only three genes for RAB11/RABA members, whereas this subgroup is extremely expanded in Arabidopsis; 26 members are encoded in its genome. This fact suggests that expansion of RAB GTPases was not simply related to terrestrialization and/or multicellularization. Further comparative analyses of RAB GTPases among various land plants should be performed for better understanding of the significance of diversification of RAB GTPases during land plant evolution.

Whereas increase in a number of RAB GTPases followed by functional differentiation would play important roles in evolution of the membrane trafficking

129

system, secondary loss of RAB GTPases should be also an important method for diversification and specialization of the membrane trafficking system (Elias et al., 2012; Klopper et al., 2012). To obtain insights into significance of secondary loss of RAB GTPases, I performed functional analyses of MpRAB21 and MpRAB23, whose homologs were secondarily lost several times independently during land plant evolution. I demonstrated that RAB21 is required for normal thallus development of *M. polymorpha*, suggesting that the reason why RAB21 was lost is not simply because it is not important for membrane trafficking. My results also indicated that post-Golgi membrane trafficking pathways have been substantially diversified among land plant lineages. Further functional analyses of this RAB group would be needed for understanding how endosomal membrane trafficking pathways have been diversified during evolution and the reason why RAB21 could be lost in some plant lineages.

The distribution of *RAB23* genes among land plants and the function of MpRAB23 strongly supports the idea that the loss of RAB23 gene is closely correlated to loss of flagella during land plant evolution. In animals, the cilium is not only a motile structure but also a sensor of environmental and developmental cues. Mainly because of essential and complex functions of cilia, the precise molecular function of RAB23 in formation of flagella and cilia has still been ambiguous in animals. Analyses of RAB23 functions in formation and functions of flagellar using plant spermatozoids should be quite effective and informative to understand the basic function of the RAB23 group. I also demonstrated that MpRAB23 also plays important roles in formation of a plant-specific structure, the MLS. Previous electron microscopic analyses indicated that the MLS is a distinctive structure in spermatozoids, however, how the MLS is organized is still unknown. Clarification of the relationship between RAB23 function and the MLS

organization would lead us to understanding how this plant-unique microtubule-containing structure was acquired during evolution.

This study demonstrated that *M. polymorpha* has a simple but unique membrane trafficking system, which would be a sound system for analysis of diversification and evolution of the membrane trafficking system. This system would be also suitable for unraveling the fundamental functions of conserved machinery components such as RAB21 and RAB23. Moreover, *M. polymorpha* would be an ideal system to understand the significance of secondary loss of RAB GTPase in diversification of membrane trafficking system. Similar approaches could be also applied for other biological functions and gene families than membrane trafficking and RAB GTPases. *M. polymorpha* is a classical research target of botany, which was already described in literatures in ancient Greece. Now the new era of *M. polymorpha* studies has opened, which could be called the Renaissance of *M. polymorpha* by future generations of plant scientists.

References

Althoff, F., Kopischke, S., Zobell, O., Ide, K., Ishizaki, K., Kohchi, T., et al. (2014) Comparison of the MpEF1alpha and CaMV35 promoters for application in *Marchantia polymorpha* overexpression studies. *Transgenic Res.* 23: 235-244.

Amborella Genome, P. (2013) The Amborella genome and the evolution of flowering plants. *Science.* 342: 1241089.

Asaoka, R., Uemura, T., Ito, J., Fujimoto, M., Ito, E., Ueda, T., et al. (2013) Arabidopsis RABA1 GTPases are involved in transport between the trans-Golgi network and the plasma membrane, and are required for salinity stress tolerance. *Plant J.* 73: 240-249.

Banks, J.A., Nishiyama, T., Hasebe, M., Bowman, J.L., Gribskov, M., dePamphilis, C., et al. (2011) The Selaginella genome identifies genetic changes associated with the evolution of vascular plants. *Science.* 332: 960-963.

Batoko, H., Zheng, H.Q., Hawes, C. and Moore, I. (2000) A rab1 GTPase is required for transport between the endoplasmic reticulum and golgi apparatus and for normal golgi movement in plants. *Plant Cell.* 12: 2201-2218.

Benkova, E., Michniewicz, M., Sauer, M., Teichmann, T., Seifertova, D., Jurgens, G., et al. (2003) Local, efflux-dependent auxin gradients as a common module for plant organ formation. *Cell.* 115: 591-602.

Bischler, H. (1986) *Marchantia polymorpha* L. s. lat. karyotype analysis. *Jurnal of the Hattori Botanical Laboratory.* 60: 105-117.

Blanc, G., Agarkova, I., Grimwood, J., Kuo, A., Brueggeman, A., Dunigan, D.D., et al. (2012) The genome of the polar eukaryotic microalga *Coccomyxa subellipsoidea* reveals traits of cold adaptation. *Genome Biol.* 13: R39.

Boehlke, C., Bashkurov, M., Buescher, A., Krick, T., John, A.K., Nitschke, R., et al.

(2010) Differential role of Rab proteins in ciliary trafficking: Rab23 regulates smoothened levels. *J Cell Sci.* 123: 1460-1467.

Bowman, J.L., Kohchi, T., Yamato, K.T., Jenkins, J., Shu, S., Ishizaki, K., et al. (2017) Insights into Land Plant Evolution Garnered from the *Marchantia polymorpha* Genome. *Cell.* 171: 287-304 e215.

Burgo, A., Proux-Gillardeaux, V., Sotirakis, E., Bun, P., Casano, A., Verraes, A., et al. (2012) A molecular network for the transport of the TI-VAMP/VAMP7 vesicles from cell center to periphery. *Dev Cell.* 23: 166-180.

Burgo, A., Sotirakis, E., Simmler, M.C., Verraes, A., Chamot, C., Simpson, J.C., et al. (2009) Role of Varp, a Rab21 exchange factor and TI-VAMP/VAMP7 partner, in neurite growth. *EMBO Rep.* 10: 1117-1124.

Buschmann, H., Holtmannspotter, M., Borchers, A., O'Donoghue, M.T. and Zachgo, S. (2016) Microtubule dynamics of the centrosome-like polar organizers from the basal land plant *Marchantia polymorpha. New Phytol.* 209: 999-1013.

Carothers, Z.B. and Kreitner, G.L. (1968) Studies of spermatogenesis in the Hepaticae. II. Blepharoplast structure in the spermatid of Marchantia. *J Cell Biol.* 36: 603-616.

Carvalho-Santos, Z., Azimzadeh, J., Pereira-Leal, J.B. and Bettencourt-Dias, M. (2011) Evolution: Tracing the origins of centrioles, cilia, and flagella. *J Cell Biol.* 194: 165-175.

Cheung, A.Y. (2002) Rab2 GTPase Regulates Vesicle Trafficking between the Endoplasmic Reticulum and the Golgi Bodies and Is Important to Pollen Tube Growth. *The Plant Cell Online.* 14: 945-962.

Chiyoda, S., Ishizaki, K., Kataoka, H., Yamato, K.T. and Kohchi, T. (2008) Direct transformation of the liverwort *Marchantia polymorpha* L. by particle bombardment

using immature thalli developing from spores. *Plant Cell Rep.* 27: 1467-1473.

Choi, S.W., Tamaki, T., Ebine, K., Uemura, T., Ueda, T. and Nakano, A. (2013) RABA members act in distinct steps of subcellular trafficking of the FLAGELLIN SENSING2 receptor. *Plant Cell.* 25: 1174-1187.

Chow, C.M., Neto, H., Foucart, C. and Moore, I. (2008) Rab-A2 and Rab-A3 GTPases define a trans-golgi endosomal membrane domain in Arabidopsis that contributes substantially to the cell plate. *Plant Cell.* 20: 101-123.

Dacks, J.B. and Field, M.C. (2007) Evolution of the eukaryotic membrane-trafficking system: origin, tempo and mode. *J Cell Sci.* 120: 2977-2985.

de Graaf, B.H., Cheung, A.Y., Andreyeva, T., Levasseur, K., Kieliszewski, M. and Wu, H.M. (2005) Rab11 GTPase-regulated membrane trafficking is crucial for tip-focused pollen tube growth in tobacco. *Plant Cell.* 17: 2564-2579.

Deane, J.A., Cole, D.G., Seeley, E.S., Diener, D.R. and Rosenbaum, J.L. (2001) Localization of intraflagellar transport protein IFT52 identifies basal body transitional fibers as the docking site for IFT particles. *Curr Biol.* 11: 1586-1590.

Derelle, E., Ferraz, C., Rombauts, S., Rouze, P., Worden, A.Z., Robbens, S., et al. (2006) Genome analysis of the smallest free-living eukaryote Ostreococcus tauri unveils many unique features. *Proc Natl Acad Sci U S A.* 103: 11647-11652.

Dhonukshe, P., Aniento, F., Hwang, I., Robinson, D.G., Mravec, J., Stierhof, Y.D., et al. (2007) Clathrin-mediated constitutive endocytosis of PIN auxin efflux carriers in Arabidopsis. *Curr Biol.* 17: 520-527.

Dishinger, J.F., Kee, H.L., Jenkins, P.M., Fan, S., Hurd, T.W., Hammond, J.W., et al. (2010) Ciliary entry of the kinesin-2 motor KIF17 is regulated by importin-beta2 and RanGTP. *Nat Cell Biol.* 12: 703-710.

Doelling, J.H., Walker, J.M., Friedman, E.M., Thompson, A.R. and Vierstra, R.D. (2002) The APG8/12-activating enzyme APG7 is required for proper nutrient recycling and senescence in *Arabidopsis thaliana*. *J Biol Chem.* 277: 33105-33114.

Ebine, K., Fujimoto, M., Okatani, Y., Nishiyama, T., Goh, T., Ito, E., et al. (2011) A membrane trafficking pathway regulated by the plant-specific RAB GTPase ARA6. *Nat Cell Biol.* 13: 853-859.

Edgar, R.C. (2004) MUSCLE: multiple sequence alignment with high accuracy and high throughput. *Nucleic Acids Res.* 32: 1792-1797.

Eggenschwiler, J.T., Espinoza, E. and Anderson, K.V. (2001) Rab23 is an essential negative regulator of the mouse Sonic hedgehog signalling pathway. *Nature.* 412: 194-198.

Eklund, D.M., Ishizaki, K., Flores-Sandoval, E., Kikuchi, S., Takebayashi, Y., Tsukamoto, S., et al. (2015) Auxin Produced by the Indole-3-Pyruvic Acid Pathway Regulates Development and Gemmae Dormancy in the Liverwort *Marchantia polymorpha*. *Plant Cell.* 27: 1650-1669.

Elias, M., Brighouse, A., Gabernet-Castello, C., Field, M.C. and Dacks, J.B. (2012) Sculpting the endomembrane system in deep time: high resolution phylogenetics of Rab GTPases. *J Cell Sci.* 125: 2500-2508.

Era, A. (2012) Studies of membrane trafficking system of the basal land plant, *Marchantia polymorpha*. *Doctoral thesis (The University of Tokyo)*.

Friml, J., Vieten, A., Sauer, M., Weijers, D., Schwarz, H., Hamann, T., et al. (2003) Efflux-dependent auxin gradients establish the apical-basal axis of Arabidopsis. *Nature.* 426: 147-153.

Fujimoto, M. and Ueda, T. (2012) Conserved and plant-unique mechanisms regulating

plant post-Golgi traffic. *Front Plant Sci.* 3: 197.

Geldner, N., Anders, N., Wolters, H., Keicher, J., Kornberger, W., Muller, P., et al. (2003) The Arabidopsis GNOM ARF-GEF mediates endosomal recycling, auxin transport, and auxin-dependent plant growth. *Cell.* 112: 219-230.

Gendre, D., Oh, J., Boutte, Y., Best, J.G., Samuels, L., Nilsson, R., et al. (2011) Conserved Arabidopsis ECHIDNA protein mediates trans-Golgi-network trafficking and cell elongation. *Proc Natl Acad Sci U S A.* 108: 8048-8053.

Goh, T., Uchida, W., Arakawa, S., Ito, E., Dainobu, T., Ebine, K., et al. (2007) VPS9a, the common activator for two distinct types of Rab5 GTPases, is essential for the development of *Arabidopsis thaliana*. *Plant Cell.* 19: 3504-3515.

Goldfarb, D.S., Corbett, A.H., Mason, D.A., Harreman, M.T. and Adam, S.A. (2004) Importin alpha: a multipurpose nuclear-transport receptor. *Trends Cell Biol.* 14: 505-514.

Graham, L.E. and McBride, G.E. (1979) The occurrence and phylogenetic significance of a multilayered structure in Coleochaete spermatozoids. *Am J Bot.* 66: 887-894.

Grosshans, B.L., Ortiz, D. and Novick, P. (2006) Rabs and their effectors: achieving specificity in membrane traffic. *Proc Natl Acad Sci U S A.* 103: 11821-11827.

Guan, R., Zhao, Y., Zhang, H., Fan, G., Liu, X., Zhou, W., et al. (2016) Draft genome of the living fossil *Ginkgo biloba*. *Gigascience.* 5: 49.

Hanamata, S., Kurusu, T. and Kuchitsu, K. (2014) Roles of autophagy in male reproductive development in plants. *Front Plant Sci.* 5: 457.

Hanaoka, H., Noda, T., Shirano, Y., Kato, T., Hayashi, H., Shibata, D., et al. (2002) Leaf senescence and starvation-induced chlorosis are accelerated by the disruption of an Arabidopsis autophagy gene. *Plant Physiol.* 129: 1181-1193.

Hatsugai, N., Iwasaki, S., Tamura, K., Kondo, M., Fuji, K., Ogasawara, K., et al. (2009) A novel membrane fusion-mediated plant immunity against bacterial pathogens. *Genes Dev.* 23: 2496-2506.

Henne, W.M., Buchkovich, N.J. and Emr, S.D. (2011) The ESCRT pathway. *Dev Cell.* 21: 77-91.

Heucken, N. and Ivanov, R. (2017) The retromer, sorting nexins and the plant endomembrane protein trafficking. *J Cell Sci.*

Higo, A., Niwa, M., Yamato, K.T., Yamada, L., Sawada, H., Sakamoto, T., et al. (2016) Transcriptional Framework of Male Gametogenesis in the Liverwort *Marchantia polymorpha* L. *Plant Cell Physiol.* 57: 325-338.

Hori, K., Maruyama, F., Fujisawa, T., Togashi, T., Yamamoto, N., Seo, M., et al. (2014) *Klebsormidium flaccidum* genome reveals primary factors for plant terrestrial adaptation. *Nat Commun.* 5: 3978.

Horiuchi, H., Lippe, R., McBride, H.M., Rubino, M., Woodman, P., Stenmark, H., et al. (1997) A novel Rab5 GDP/GTP exchange factor complexed to Rabaptin-5 links nucleotide exchange to effector recruitment and function. *Cell.* 90: 1149-1159.

Hutagalung, A.H. and Novick, P.J. (2011) Role of Rab GTPases in membrane traffic and cell physiology. *Physiol Rev.* 91: 119-149.

International Brachypodium, I. (2010) Genome sequencing and analysis of the model grass *Brachypodium distachyon*. *Nature.* 463: 763-768.

Ishizaki, K., Chiyoda, S., Yamato, K.T. and Kohchi, T. (2008) Agrobacterium-mediated transformation of the haploid liverwort *Marchantia polymorpha* L., an emerging model for plant biology. *Plant Cell Physiol.* 49: 1084-1091.

Ishizaki, K., Johzuka-Hisatomi, Y., Ishida, S., Iida, S. and Kohchi, T. (2013) Homologous

recombination-mediated gene targeting in the liverwort *Marchantia polymorpha* L. *Sci Rep.* 3: 1532.

Ishizaki, K., Nishihama, R., Ueda, M., Inoue, K., Ishida, S., Nishimura, Y., et al. (2015) Development of Gateway Binary Vector Series with Four Different Selection Markers for the Liverwort *Marchantia polymorpha. PLoS One.* 10: e0138876.

Ivanov, R., Brumbarova, T., Blum, A., Jantke, A.M., Fink-Straube, C. and Bauer, P. (2014) SORTING NEXIN1 is required for modulating the trafficking and stability of the Arabidopsis IRON-REGULATED TRANSPORTER1. *Plant Cell.* 26: 1294-1307.

Jaillais, Y., Santambrogio, M., Rozier, F., Fobis-Loisy, I., Miege, C. and Gaude, T. (2007) The retromer protein VPS29 links cell polarity and organ initiation in plants. *Cell.* 130: 1057-1070.

Johansen, J.N., Chow, C.M., Moore, I. and Hawes, C. (2009) AtRAB-H1b and AtRAB-H1c GTPases, homologues of the yeast Ypt6, target reporter proteins to the Golgi when expressed in Nicotiana tabacum and *Arabidopsis thaliana. J Exp Bot.* 60: 3179-3193.

Ju, C., Van de Poel, B., Cooper, E.D., Thierer, J.H., Gibbons, T.R., Delwiche, C.F., et al. (2015) Conservation of ethylene as a plant hormone over 450 million years of evolution. *Nat Plants.* 1: 14004.

Kanazawa, T. (2016) Studies on diversification of organelles and membrane trafficking pathways using *Marchantia polymorpha. Doctoral thesis (The University of Tokyo).*

Kanazawa, T., Era, A., Minamino, N., Shikano, Y., Fujimoto, M., Uemura, T., et al. (2016) SNARE Molecules in *Marchantia polymorpha*: Unique and Conserved Features of the Membrane Fusion Machinery. *Plant Cell Physiol.* 57: 307-324.

Kanazawa, T., Ishizaki, K., Kohchi, T., Hanaoka, M. and Tanaka, K. (2013)

Characterization of four nuclear-encoded plastid RNA polymerase sigma factor genes in the liverwort *Marchantia polymorpha*: blue-light- and multiple stress-responsive SIG5 was acquired early in the emergence of terrestrial plants. *Plant Cell Physiol.* 54: 1736-1748.

Kang, H., Kim, S.Y., Song, K., Sohn, E.J., Lee, Y., Lee, D.W., et al. (2012) Trafficking of vacuolar proteins: the crucial role of Arabidopsis vacuolar protein sorting 29 in recycling vacuolar sorting receptor. *Plant Cell.* 24: 5058-5073.

Kato, H., Ishizaki, K., Kouno, M., Shirakawa, M., Bowman, J.L., Nishihama, R., et al. (2015) Auxin-Mediated Transcriptional System with a Minimal Set of Components Is Critical for Morphogenesis through the Life Cycle in *Marchantia polymorpha*. *PLoS Genet.* 11: e1005084.

Kato, H., Kouno, M., Takeda, M., Suzuki, H., Ishizaki, K., Nishihama, R., et al. (2017) The Roles of the Sole Activator-Type Auxin Response Factor in Pattern Formation of *Marchantia polymorpha*. *Plant Cell Physiol.* 58: 1642-1651.

Kawahara, Y., de la Bastide, M., Hamilton, J.P., Kanamori, H., McCombie, W.R., Ouyang, S., et al. (2013) Improvement of the Oryza sativa Nipponbare reference genome using next generation sequence and optical map data. *Rice (N Y).* 6: 4.

Kim, Y.H., Han, M.E. and Oh, S.O. (2017) The molecular mechanism for nuclear transport and its application. *Anat Cell Biol.* 50: 77-85.

Kirchhelle, C., Chow, C.M., Foucart, C., Neto, H., Stierhof, Y.D., Kalde, M., et al. (2016) The Specification of Geometric Edges by a Plant Rab GTPase Is an Essential Cell-Patterning Principle During Organogenesis in Arabidopsis. *Dev Cell.* 36: 386-400.

Kleine-Vehn, J., Leitner, J., Zwiewka, M., Sauer, M., Abas, L., Luschnig, C., et al. (2008) Differential degradation of PIN2 auxin efflux carrier by retromer-dependent vacuolar

targeting. *Proc Natl Acad Sci U S A.* 105: 17812-17817.

Klopper, T.H., Kienle, N., Fasshauer, D. and Munro, S. (2012) Untangling the evolution

of Rab G proteins: implications of a comprehensive genomic analysis. *BMC Biol.* 10:

71.

Kotzer, A.M., Brandizzi, F., Neumann, U., Paris, N., Moore, I. and Hawes, C. (2004)

AtRabF2b (Ara7) acts on the vacuolar trafficking pathway in tobacco leaf epidermal

cells. *J Cell Sci.* 117: 6377-6389.

Kubota, A., Ishizaki, K., Hosaka, M. and Kohchi, T. (2013) Efficient Agrobacterium-

mediated transformation of the liverwort *Marchantia polymorpha* using regenerating

thalli. *Biosci Biotechnol Biochem.* 77: 167-172.

Kurusu, T., Koyano, T., Hanamata, S., Kubo, T., Noguchi, Y., Yagi, C., et al. (2014)

OsATG7 is required for autophagy-dependent lipid metabolism in rice postmeiotic

anther development. *Autophagy.* 10: 878-888.

Kushnirov, V.V. (2000) Rapid and reliable protein extraction from yeast. *Yeast.* 16: 857-

860.

Lai, Z., Wang, F., Zheng, Z., Fan, B. and Chen, Z. (2011) A critical role of autophagy in

plant resistance to necrotrophic fungal pathogens. *Plant J.* 66: 953-968.

Leaf, A. and Von Zastrow, M. (2015) Dopamine receptors reveal an essential role of IFT-

B, KIF17, and Rab23 in delivering specific receptors to primary cilia. *Elife.* 4.

Li, Y., Wang, F.H. and Knox, R.B. (1989) Ultrastructural Analysis of the Flagellar

Apparatus in Sperm Cells of *Ginkgo-Biloba. Protoplasma.* 149: 57-63.

Lim, Y.S. and Tang, B.L. (2015) A role for Rab23 in the trafficking of Kif17 to the primary

cilium. *J Cell Sci.* 128: 2996-3008.

Liu, Y., Xiong, Y. and Bassham, D.C. (2014) Autophagy is required for tolerance of

drought and salt stress in plants. *Autophagy.* 5: 954-963.

Lumb, J.H. and Field, M.C. (2011) Rab23 is a flagellar protein in *Trypanosoma brucei*. *BMC Res Notes.* 4: 190.

Merchant, S.S., Prochnik, S.E., Vallon, O., Harris, E.H., Karpowicz, S.J., Witman, G.B., et al. (2007) The Chlamydomonas genome reveals the evolution of key animal and plant functions. *Science.* 318: 245-250.

Minamino, N., Kanazawa, T., Nishihama, R., Yamato, K.T., Ishizaki, K., Kohchi, T., et al. (2017) Dynamic reorganization of the endomembrane system during spermatogenesis in *Marchantia polymorpha*. *J Plant Res.* 130: 433-441.

Ming, R., VanBuren, R., Liu, Y., Yang, M., Han, Y., Li, L.T., et al. (2013) Genome of the long-living sacred lotus (*Nelumbo nucifera* Gaertn.). *Genome Biol.* 14: R41.

Mizushima, N. and Komatsu, M. (2011) Autophagy: renovation of cells and tissues. *Cell.* 147: 728-741.

Nakatogawa, H., Suzuki, K., Kamada, Y. and Ohsumi, Y. (2009) Dynamics and diversity in autophagy mechanisms: lessons from yeast. *Nat Rev Mol Cell Biol.* 10: 458-467.

Nishihama, R., Ishida, S., Urawa, H., Kamei, Y. and Kohchi, T. (2016) Conditional Gene Expression/Deletion Systems for Marchantia polymorpha Using its Own Heat-Shock Promoter and Cre/loxP-Mediated Site-Specific Recombination. *Plant Cell Physiol.* 57: 271-280.

O'Donnell, L., Nicholls, P.K., O'Bryan, M.K., McLachlan, R.I. and Stanton, P.G. (2011) Spermiation: The process of sperm release. *Spermatogenesis.* 1: 14-35.

Ohtaka, K., Hori, K., Kanno, Y., Seo, M. and Ohta, H. (2017) Primitive Auxin Response without TIR1 and Aux/IAA in the Charophyte Alga *Klebsormidium nitens*. *Plant Physiol.* 174: 1621-1632.

Pellinen, T., Arjonen, A., Vuoriluoto, K., Kallio, K., Fransen, J.A. and Ivaska, J. (2006) Small GTPase Rab21 regulates cell adhesion and controls endosomal traffic of beta1-integrins. *J Cell Biol.* 173: 767-780.

Pellinen, T., Tuomi, S., Arjonen, A., Wolf, M., Edgren, H., Meyer, H., et al. (2008) Integrin trafficking regulated by Rab21 is necessary for cytokinesis. *Dev Cell.* 15: 371-385.

Pinheiro, H., Samalova, M., Geldner, N., Chory, J., Martinez, A. and Moore, I. (2009) Genetic evidence that the higher plant Rab-D1 and Rab-D2 GTPases exhibit distinct but overlapping interactions in the early secretory pathway. *J Cell Sci.* 122: 3749-3758.

Preuss, M.L., Serna, J., Falbel, T.G., Bednarek, S.Y. and Nielsen, E. (2004) The Arabidopsis Rab GTPase RabA4b localizes to the tips of growing root hair cells. *Plant Cell.* 16: 1589-1603.

Qi, X. and Zheng, H. (2013) Rab-A1c GTPase defines a population of the trans-Golgi network that is sensitive to endosidin1 during cytokinesis in Arabidopsis. *Mol Plant.* 6: 847-859.

Rensing, S.A., Ick, J., Fawcett, J.A., Lang, D., Zimmer, A., Van de Peer, Y., et al. (2007) An ancient genome duplication contributed to the abundance of metabolic genes in the moss *Physcomitrella patens*. *BMC Evol Biol.* 7: 130.

Rensing, S.A., Lang, D., Zimmer, A.D., Terry, A., Salamov, A., Shapiro, H., et al. (2008) The Physcomitrella genome reveals evolutionary insights into the conquest of land by plants. *Science.* 319: 64-69.

Renzaglia, K.S. and Duckett, J.G. (1987) Spermatogenesis in *Blasia pusilla*: From Young Antheridium through Mature Spermatozoid. *The Bryologist.* 90: 419.

Renzaglia, K.S. and Garbary, D.J. (2001) Motile Gametes of Land Plants: Diversity, Development, and Evolution. *Critical Reviews in Plant Sciences.* 20: 107-213.

Rutherford, S. and Moore, I. (2002) The Arabidopsis Rab GTPase family: another enigma variation. *Curr Opin Plant Biol.* 5: 518-528.

Saito, C. and Ueda, T. (2009) Chapter 4: functions of RAB and SNARE proteins in plant life. *Int Rev Cell Mol Biol.* 274: 183-233.

Saito, K., Murai, J., Kajiho, H., Kontani, K., Kurosu, H. and Katada, T. (2002) A novel binding protein composed of homophilic tetramer exhibits unique properties for the small GTPase Rab5. *J Biol Chem.* 277: 3412-3418.

Sakai, H., Lee, S.S., Tanaka, T., Numa, H., Kim, J., Kawahara, Y., et al. (2013) Rice Annotation Project Database (RAP-DB): an integrative and interactive database for rice genomics. *Plant Cell Physiol.* 54: e6.

Sakurai, H.T., Inoue, T., Nakano, A. and Ueda, T. (2016) ENDOSOMAL RAB EFFECTOR WITH PX-DOMAIN, an Interacting Partner of RAB5 GTPases, Regulates Membrane Trafficking to Protein Storage Vacuoles in Arabidopsis. *Plant Cell.* 28: 1490-1503.

Sanchez-Vera, V., Kenchappa, C.S., Landberg, K., Bressendorff, S., Schwarzbach, S., Martin, T., et al. (2017) Autophagy is required for gamete differentiation in the moss *Physcomitrella patens. Autophagy.* 13: 1939-1951.

Sanderfoot, A. (2007) Increases in the number of SNARE genes parallels the rise of multicellularity among the green plants. *Plant Physiol.* 144: 6-17.

Saraste, J., Lahtinen, U. and Goud, B. (1995) Localization of the small GTP-binding protein rab1p to early compartments of the secretory pathway. *J Cell Sci.* 108 (Pt 4): 1541-1552.

Schnable, P.S., Ware, D., Fulton, R.S., Stein, J.C., Wei, F., Pasternak, S., et al. (2009) The

    B73 maize genome: complexity, diversity, and dynamics. *Science.* 326: 1112-1115.

Shimada, T., Koumoto, Y., Li, L., Yamazaki, M., Kondo, M., Nishimura, M., et al. (2006)

    AtVPS29, a putative component of a retromer complex, is required for the efficient

    sorting of seed storage proteins. *Plant Cell Physiol.* 47: 1187-1194.

Shimamura, M. (2016) *Marchantia polymorpha*: Taxonomy, Phylogeny and Morphology

    of a Model System. *Plant Cell Physiol.* 57: 230-256.

Shimamura, M., Brown, R.C., Lemmon, B.E., Akashi, T., Mizuno, K., Nishihara, N., et

    al. (2004) Gamma-tubulin in basal land plants: characterization, localization, and

    implication in the evolution of acentriolar microtubule organizing centers. *Plant Cell.*

    16: 45-59.

Simpson, J.C., Griffiths, G., Wessling-Resnick, M., Fransen, J.A., Bennett, H. and Jones,

    A.T. (2004) A role for the small GTPase Rab21 in the early endocytic pathway. *J Cell*

    Sci. 117: 6297-6311.

Sohn, E.J., Kim, E.S., Zhao, M., Kim, S.J., Kim, H., Kim, Y.W., et al. (2003) Rha1, an

    Arabidopsis Rab5 homolog, plays a critical role in the vacuolar trafficking of soluble

    cargo proteins. *Plant Cell.* 15: 1057-1070.

Speth, E.B., Imboden, L., Hauck, P. and He, S.Y. (2009) Subcellular localization and

    functional analysis of the Arabidopsis GTPase RabE. *Plant Physiol.* 149: 1824-1837.

Sugano, S.S., Shirakawa, M., Takagi, J., Matsuda, Y., Shimada, T., Hara-Nishimura, I., et

    al. (2014) CRISPR/Cas9-mediated targeted mutagenesis in the liverwort *Marchantia*

    polymorpha L. *Plant Cell Physiol.* 55: 475-481.

Suire, C., Bouvier, F., Backhaus, R.A., Begu, D., Bonneu, M. and Camara, B. (2000)

    Cellular localization of isoprenoid biosynthetic enzymes in *Marchantia polymorpha*.

Uncovering a new role of oil bodies. *Plant Physiol.* 124: 971-978.

Sunada, M. (2015) Studies on activation mechanism of two types RAB5 in *Arabidopsis thaliana*. *Doctoral thesis (The University of Tokyo).*

Sunada, M., Goh, T., Ueda, T. and Nakano, A. (2016) Functional analyses of the plant-specific C-terminal region of VPS9a: the activating factor for RAB5 in *Arabidopsis thaliana*. *J Plant Res.* 129: 93-102.

Szymanska, K. and Johnson, C.A. (2012) The transition zone: an essential functional compartment of cilia. *Cilia.* 1: 10.

Tanaka, M., Esaki, T., Kenmoku, H., Koeduka, T., Kiyoyama, Y., Masujima, T., et al. (2016) Direct evidence of specific localization of sesquiterpenes and marchantin A in oil body cells of *Marchantia polymorpha* L. *Phytochemistry.* 130: 77-84.

Taschner, M., Bhogaraju, S. and Lorentzen, E. (2012) Architecture and function of IFT complex proteins in ciliogenesis. *Differentiation.* 83: S12-22.

Ueda, K. (1979) Denshikenbikyou de Mita Syokubutsu no Kouzou. Baishukan, Tokyo.

Ueda, T., Anai, T., Tsukaya, H., Hirata, A. and Uchimiya, H. (1996) Characterization and subcellular localization of a small GTP-binding protein (Ara-4) from Arabidopsis: conditional expression under control of the promoter of the gene for heat-shock protein HSP81-1. *Mol Gen Genet.* 250: 533-539.

Ueda, T., Uemura, T., Sato, M.H. and Nakano, A. (2004) Functional differentiation of endosomes in Arabidopsis cells. *Plant J.* 40: 783-789.

Ueda, T., Yamaguchi, M., Uchimiya, H. and Nakano, A. (2001) Ara6, a plant-unique novel type Rab GTPase, functions in the endocytic pathway of *Arabidopsis thaliana*. *EMBO J.* 20: 4730-4741.

Uemura, T., Kim, H., Saito, C., Ebine, K., Ueda, T., Schulze-Lefert, P., et al. (2012) Qa-

SNAREs localized to the trans-Golgi network regulate multiple transport pathways and extracellular disease resistance in plants. *Proc Natl Acad Sci U S A.* 109: 1784-1789.

van der Sluijs, P., Zibouche, M. and van Kerkhof, P. (2013) Late steps in secretory lysosome exocytosis in cytotoxic lymphocytes. *Front Immunol.* 4: 359.

Vaughn, K.C. and Renzaglia, K.S. (2006) Structural and immunocytochemical characterization of the *Ginkgo biloba* L. sperm motility apparatus. *Protoplasma.* 227: 165-173.

Wheeler, R.J., Gluenz, E. and Gull, K. (2015) Basal body multipotency and axonemal remodelling are two pathways to a 9+0 flagellum. *Nat Commun.* 6: 8964.

Yamazaki, M., Shimada, T., Takahashi, H., Tamura, K., Kondo, M., Nishimura, M., et al. (2008) Arabidopsis VPS35, a retromer component, is required for vacuolar protein sorting and involved in plant growth and leaf senescence. *Plant Cell Physiol.* 49: 142-156.

Yoshimoto, K. (2012) Beginning to understand autophagy, an intracellular self-degradation system in plants. *Plant Cell Physiol.* 53: 1355-1365.

Yoshimura, S., Egerer, J., Fuchs, E., Haas, A.K. and Barr, F.A. (2007) Functional dissection of Rab GTPases involved in primary cilium formation. *J Cell Biol.* 178: 363-369.

Yuan, Q., Ren, C., Xu, W., Petri, B., Zhang, J., Zhang, Y., et al. (2017) PKN1 Directs Polarized RAB21 Vesicle Trafficking via RPH3A and Is Important for Neutrophil Adhesion and Ischemia-Reperfusion Injury. *Cell Rep.* 19: 2586-2597.

Zelazny, E., Santambrogio, M., Pourcher, M., Chambrier, P., Berne-Dedieu, A., Fobis-Loisy, I., et al. (2013) Mechanisms governing the endosomal membrane recruitment

of the core retromer in Arabidopsis. *J Biol Chem.* 288: 8815-8825.

Zhang, X., He, X., Fu, X.Y. and Chang, Z. (2006) Varp is a Rab21 guanine nucleotide exchange factor and regulates endosome dynamics. *J Cell Sci.* 119: 1053-1062.

Zheng, H., Camacho, L., Wee, E., Batoko, H., Legen, J., Leaver, C.J., et al. (2005) A Rab-E GTPase mutant acts downstream of the Rab-D subclass in biosynthetic membrane traffic to the plasma membrane in tobacco leaf epidermis. *Plant Cell.* 17: 2020-2036.